Journal Pre-proof

The reversible heat effects at lithium iron phosphate- and graphite electrodes

Astrid Fagertun Gunnarshaug, Signe Kjelstrup, Dick Bedeaux, Frank Richter, Odne Stokke Burheim

PII: S0013-4686(19)32439-9

DOI: https://doi.org/10.1016/j.electacta.2019.135567

Reference: EA 135567

To appear in: *Electrochimica Acta*

Received Date: 25 June 2019

Revised Date: 22 November 2019

Accepted Date: 22 December 2019

Please cite this article as: A.F. Gunnarshaug, S. Kjelstrup, D. Bedeaux, F. Richter, O.S. Burheim, The reversible heat effects at lithium iron phosphate- and graphite electrodes, *Electrochimica Acta* (2020), doi: https://doi.org/10.1016/j.electacta.2019.135567.

The reversible heat effects at lithium iron phosphate- and graphite electrodes

Astrid Fagertun Gunnarshaug[a,*], Signe Kjelstrup[a], Dick Bedeaux[a], Frank Richter[a,1], Odne Stokke Burheim[b]

[a]PoreLab, Department of Chemistry, Norwegian University of Science and Technology, NTNU, Trondheim
[b]Department of Energy and Process Engineering, Norwegian University of Science and Technology, NTNU, Trondheim, Norway

Abstract

Lithium ion batteries are used to store and produce electric energy. During the charging- and discharging processes, net heat is released or adsorbed in the battery. Temperature is one of the most important factors for battery ageing. In this study we are seeking a fundamental understanding of one of the heat effects, the reversible heat source. The role played by local reversible heat changes is mostly overlooked. We show that, despite a small full cell battery entropy change, there are large reversible half cell heat effects of opposite signs in the lithium iron phosphate oxide and lithium graphite electrode compartments. We present for the first time the Peltier heat of the $LiFePO_4$ electrode near 0% state of charge. The results are documented by thermoelectric potentials which are measured over days to achieve a stationary state. Experiments, supported by theory, enable us to decompose two processes with different characteristic times. We report effective diffusion coefficients for $LiPF_6$, and diethyl carbonate.

Keywords: Peltier heat, Seebeck effect, Reversible heat effects, $LiFePO_4$

1. Introduction

The lithium battery is already essential for the use and development of environmental friendly technology solutions [1], and the battery must comply, also to harsh treatment. During rapid charging or discharging, there is an enhanced risk that lithium layers or grains form at the solid electrode interface [2, 3]. Such interphase growth represents an extra electric resistance in addition to the one of the electrochemical reaction, and leads to increased Joule heating during use. Increased interface temperatures are detrimental for ageing [4]. But not only irreversible heat effects are present at the electrode interface. Also reversible heat effects (see below) follow the electrochemical reaction. These can act as additional heat sources, but also sinks, and are less known. In order to better understand the battery performance, its life and safety issues, there is a need for more knowledge on the precise heat effects at solid electrolyte interfaces [5, 6]. This was also pointed out by Xia, Cao and Bi in a recent review [7]. The aim of this work is to add to that.

The reversible heat change inside the battery is given by the cell entropy change, ΔS. For a battery with lithium iron phosphate and carbon electrodes the average $T\Delta S = 18$ kJ/mol at temperature T =298 K and 0% state of charge [8]. Here Δ refers to one mole of electrons produced in the external circuit by the delocalized electrochemical reaction. The contribution to the overall value from the single electrodes, is given by the theory of non-equilibrium thermodynamics, see [9]. For an electrochemical cell:

$$T\Delta S = \pi^{c} - \pi^{a} \tag{1}$$

where π^{c} is the Peltier heat of the electode functioning as the cathode, and π^{a} is the Peltier heat of the electrode functioning as the anode. Ratkje studied the effect of the local sinks and sources on the aluminum electrolysis [10]. She showed that the local reversible heat effects were of the same magnitude as the Joule heating of the electrolyte. The use of Peltier heats in Li-ion battery modelling was mentioned already by Rao and Newman [11], but has been

*Corresponding author
Email addresses: astrid.f.gunnarshaug@ntnu.no (Astrid Fagertun Gunnarshaug), signe.kjelstrup@ntnu.no (Signe Kjelstrup), odne.s.burheim@ntnu.no (Odne Stokke Burheim)
[1]Present address: AKKA DNO GmbH Peter-Hurst Str. 1B 38444 Wolfsburg, Germany

largely unaccounted for so far, see however, Huang *et al.* [12]. In this work we report for the first time that they are surprisingly large, meaning that they may help explain the thermal signature of the battery. In addition we show the large variation in the Peltier heat with the approach to a stationary state.

The Peltier heat is defined as the heat that need be added to an electrode | electrolyte interface to keep the temperature constant when positive electric current is passing from left to right across the interface under reversible conditions. Clearly, it will be a property difficult to measure, as we must observe an incremental change in temperature at isothermal conditions. The Onsager symmetry relation in the theory of electrochemical cells, helps us to circumvent this difficulty. Thanks to that, we can measure the Seebeck coefficient of a cell with two identical electrodes, rather than the Peltier heat at one electrode. The Seebeck coefficient, ϵ, for a symmetric cell with one type of electrode is defined as

$$\epsilon_t = \left(\frac{\Delta\phi}{\Delta T}\right)_{j=0} \tag{2}$$

Subscript t refers to the time of measurement and $\Delta\phi$ is the electric potential difference over the symmetric cell. From the Onsager relation for the electrode, we have [9, 13, 14]:

$$\pi = -FT\epsilon_t \tag{3}$$

relating the Peltier heat of the electrode|electrolyte interface to the Seebeck cofficient. F is Faraday's constant.

Kuzminskii *et al.* [15] reported initial Seebeck coefficients ranging from 0.65 to 4.62 mV/K depending on the lithiated state of the Li_xTiS_2- electrodes in an electrolyte of 1 M $LiBF_4$ in γ-butyrolactone already in 1994. Black *et al.* found a Seebeck coefficient of 1 mV/K using a lithium metal electrode in a cell with 1 M $LiClO_4$ in an ethylene carbonate (EC): dimethyl carbonate (DMC) electrolyte [16], while Huang *et al.* measured a coefficient of 1.17 mV/K with lithium metal electrodes and an electrolyte of 1 M $LiPF_6$ in ethylene - and diethyl carbonate [12]. The first two *emf*s were not reported at stationary state. Huang *et al.* only reported *emf*s at a relatively stable state after two hours, thus lacking information on the approach to a stationary state, which, as we will show, contains important information.

When a cell is exposed to a temperature gradient, concentration gradients may build within the cell, and change the electric potential [17]. In the stationary state, there is a balance between the chemical and the thermal force. This state is called the Soret equilibrium. The development towards this state makes the potential time-dependent and dependent on the electrolyte composition. The electrolyte in the Li-ion battery has several components, which will move in a thermal field. The time-variation in the potential can give essential information of these compounds. An important aim of this paper is to derive such properties, first in theory and next from experiments.

These observations [15, 16, 17], clearly show that $T\Delta S$, as obtained from the temperature dependence of the cell potential, does not give a local description of heat effects in the cell. For this, we need specific knowledge of Peltier heats. Measurements so far indicate that values are large, larger than the overall value [18]. We shall find Peltier heats for two common battery electrodes, namely the the lithium iron phosphate and the carbon electrodes; $Li_xC_6 \parallel Li_xFePO_4$ (see Figure 1). We measure the Seebeck coefficient of a symmetric cell with lithium iron phosphate electrodes (see Figure 2) and compute the value of the carbon electrode from the results and knowledge of the battery entropy change. In order to eliminate possible contributions from diffusion of lithium inside the electrode [19], we have chosen to first study the fully lithiated $LiFePO_4$ electrode. This work will support and extend significantly the measurement of Huang [12] and our own preliminary results, see Richter et al. [18].

2. Theoretical derivations

We present the theory for a thermoelectric cell with identical electrodes. One purpose is to have detailed theoretical expressions for decomposition of experimental data. The reader who is mostly interested in the theoretical expressions that are used in the analysis of the results, can skip the present section (intermediate derivations) and go directly to the theory summary in Section 3.

A full exposition will be given in this section, realising that the battery community is largely unfamiliar with the use of non-equilibrium thermodynamics. This theory is needed to obtain the time-evolution of the electric signal of a battery, in terms of Peltier heats. A purpose of the paper is to give a first derivation of this expression.

A common misunderstanding in literature [20] is that the Peltier heat of an electrode is related to the entropy change of the electrode half-reaction, and that it can be found from the temperature dependence of the open circuit

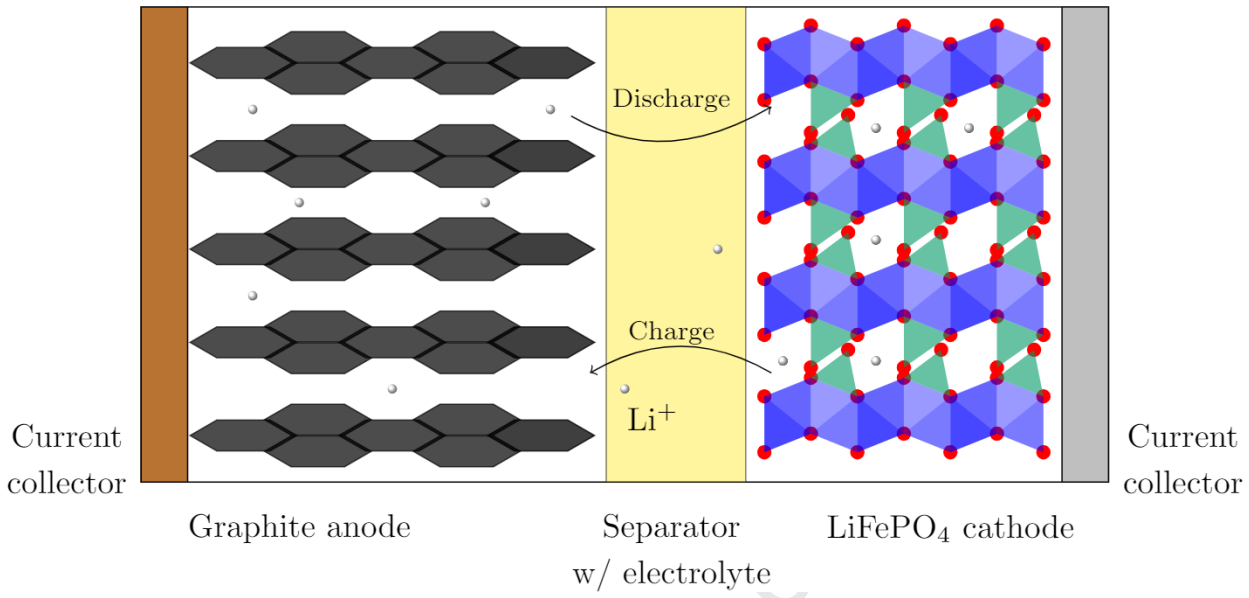

Figure 1: Cell description of a Li_xC_6 || Li_xFePO_4 battery cell.

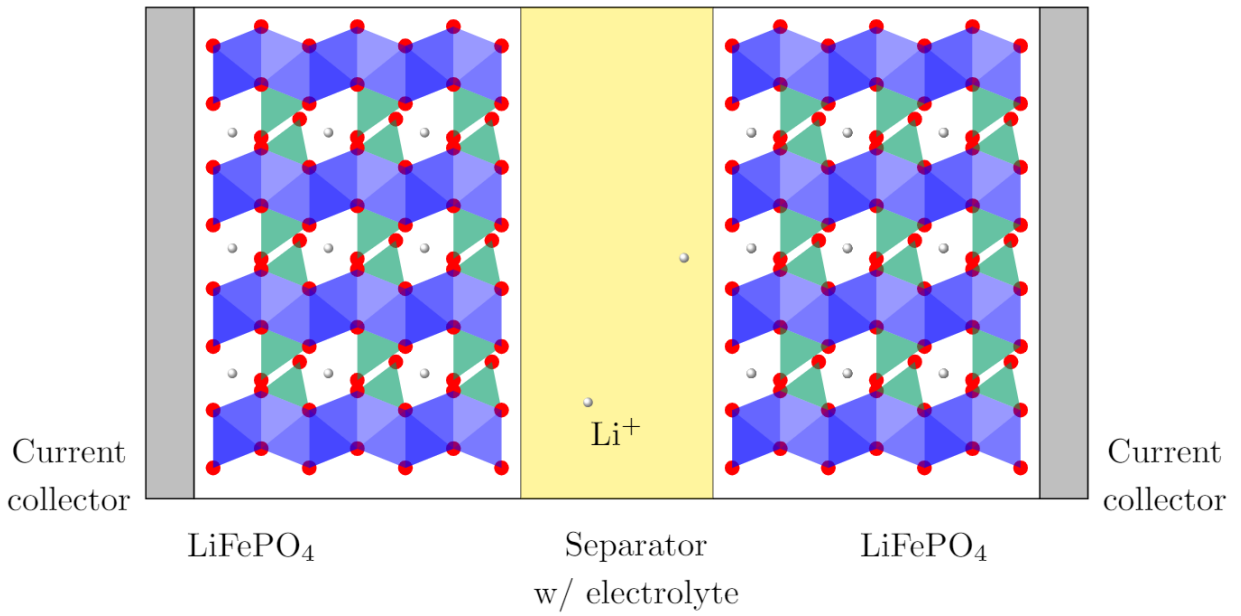

Figure 2: Cell description of the $LiFePO_4$ || $LiFePO_4$ thermocell. Both electrodes were fully lithiated.

cell potential. We will show that this is not correct. Also motivated by these misunderstandings, we give the full derivation of the cell potential, showing that the Peltier heat is defined from the open circuit potential generated by a temperature difference of a cell with identical electrodes [14, 21, 22].

2.1. The parts that make up the electrochemical cell

We divide the system presented in Figure 2 into five parts; the two electrode bulk phases, the electrolyte bulk phase and the electrode interfaces, see Figure 3. The notation for the electrode interfaces are further described in Figure 4.

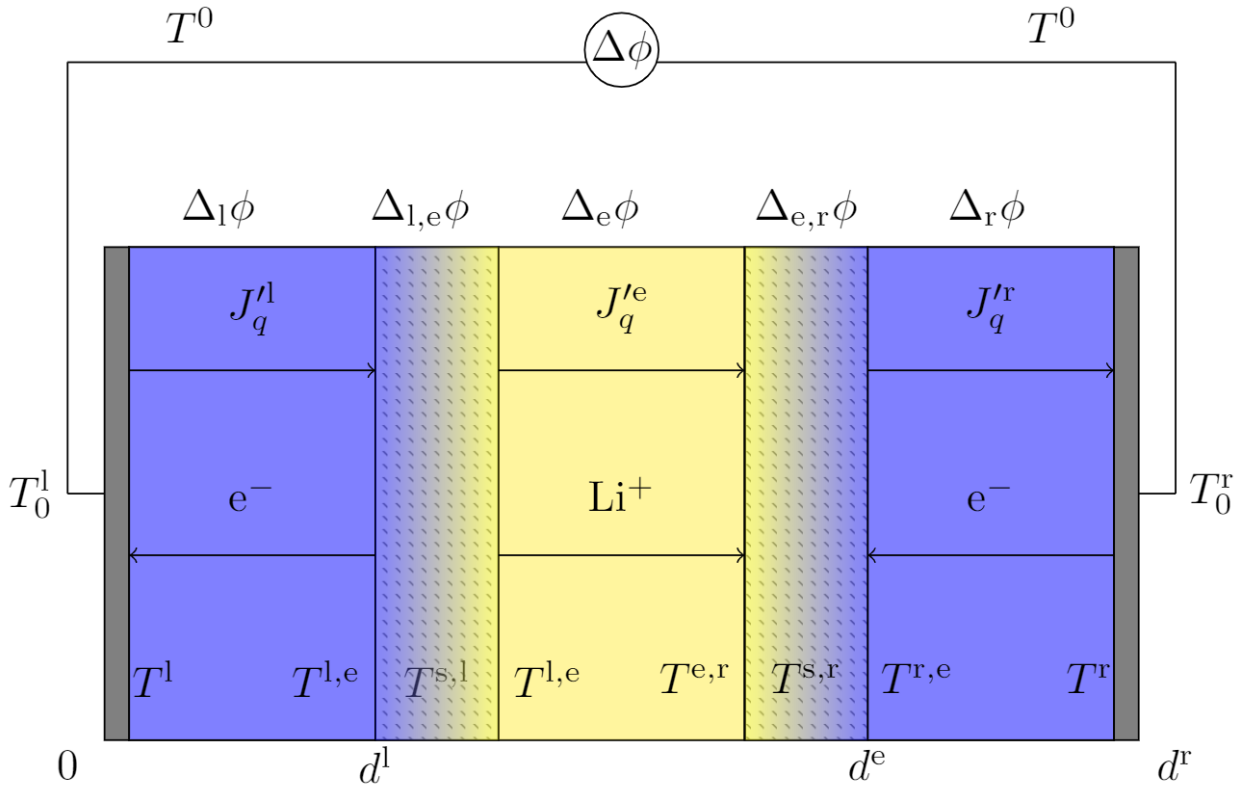

Figure 3: The thermocell in Figure 2 schematically.

The electrochemical cell in question is symmetric, and made from the same materials as lithium ion batteries. The identical electrodes are porous structures filled with electrolyte. The ternary electrolyte is contained in an (inert) separator matrix. The cell appears as a one-dimensional system, when no transport take place perpendicular to the axis between the electrodes.

The total electric potential is the sum of the contributions from the different parts:

$$\Delta_\mathrm{tot}\phi = \Delta_\mathrm{l}\phi + \Delta_\mathrm{l,e}\phi + \Delta_\mathrm{e}\phi + \Delta_\mathrm{e,r}\phi + \Delta_\mathrm{r}\phi \tag{4}$$

where l denotes the left electrode, r the right electrode, e the electrolyte and l, e and e, r the electrode surfaces. In this section, we derive the contribution from each phase to the overall potential difference. The derivation follows the same pattern. The entropy production dictates the fluxes and forces of the subsystem, and therefore the flux-force relations. Solving these, we obtain the electric potential difference as a function of temperature and time.

Due to symmetry, the theories of the two electrodes and the two electrode interfaces are the same. The theory for the separator transport is more complicated, as it contains more variables. Each subsection concludes with equations that are needed in the overall description.

2.2. Electrode bulk phases and outer circuit

The electrodes of the cell were fully lithiated $LiFePO_4$ on an aluminum backing. In the experiments, we used electrodes that were fully lithiated. This facilitates the description, because there is no driving force for diffusion within the electrode. The entropy production has heat and charge transport:

$$\sigma = J_q' \frac{\partial}{\partial x}\left(\frac{1}{T}\right) - j\frac{1}{T}\left(\frac{\partial\phi}{\partial x}\right) \tag{5}$$

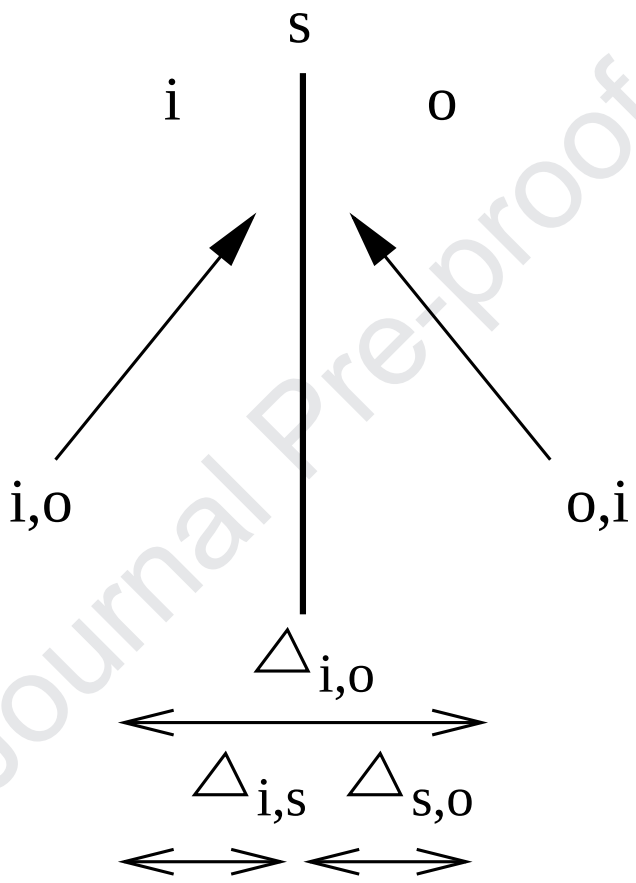

Figure 4: Notation used for transport across surfaces in the system. i denotes into the surface and o out of the surface, while s is at the surface. When dealing with either the left or right electrode in the system specifically, for the left electrode, l denotes the bulk side of the electrode and e the electrolyte bulk, and equivalently for the right electrode. Transport is defined as positive from left to right in the system. Figure reproduced with permission from [14].

where J'_q is the measurable heat flux and j is the current density. The corresponding flux equations are:

$$\begin{aligned} J'_q &= L_{qq}\left(\frac{\partial}{\partial x}\frac{1}{T}\right) + L_{q\phi}\left(-\frac{1}{T}\frac{\partial \phi}{\partial x}\right) \\ j &= L_{\phi q}\left(\frac{\partial}{\partial x}\frac{1}{T}\right) + L_{\phi\phi}\left(-\frac{1}{T}\frac{\partial \phi}{\partial x}\right) \end{aligned} \tag{6}$$

where L_{ij} is the coupling coefficient between flux i and j and the Onsager reciprocal relation holds. The following definitions for the electrode bulk phases are made:

$$\pi = F\left(\frac{J'_q}{j}\right)_{dT=0} = F\frac{L_{q\phi}}{L_{\phi\phi}} = -TS^*_{\mathrm{e}^-} \tag{7}$$

$$\lambda = -\left(\frac{J'_q}{\partial T/\partial x}\right)_{j=0} = \frac{1}{T^2}\left(L_{qq} - \frac{L^2_{q\phi}}{L_{\phi\phi}}\right) \tag{8}$$

$$r = -\left(\frac{\partial \phi/\partial x}{j}\right)_{dT=0} = \frac{T}{L_{\phi\phi}} \tag{9}$$

Here π is the Peltier coefficient of the electrodes, $S^*_{\mathrm{e}^-}$ is the transported entropy of the electrons in the electrode, a combination of that within $LiFePO_4$ and aluminum, λ is the thermal conductivity and r is the omhic resistivity of the electrode material. The intercalated lithium is in contact with an aluminum foil, which connects the electrodes to the potentiometer. The outer circuit is at constant temperature T_0. For the part of the aluminum current collectors going out of the cell, the temperatures are $T^{\mathrm{l}}_0 = T^{\mathrm{r}}_0 = T_0$. The following expressions for the temperature and electric potential gradients apply:

$$\frac{\partial T}{\partial x} = -\frac{1}{\lambda}\left(J'_q - \frac{\pi}{F}j\right) \tag{10}$$

$$\frac{\partial \phi}{\partial x} = -\frac{\pi}{TF}\frac{\partial T}{\partial x} - rj \tag{11}$$

The Seebeck coefficient is measured at open circuit, i.e. $j = 0$, so the last terms disappear, giving

$$\frac{\partial T}{\partial x} = -\frac{1}{\lambda}J'_q \tag{12}$$

$$\frac{\partial \phi}{\partial x} = -\frac{\pi}{TF}\frac{\partial T}{\partial x} \tag{13}$$

Integrating the electric potential from the surroundings at $x = 0$ to $x = d^{\mathrm{l}}$ for the left electrode and from $x = d^{\mathrm{e}}$ to the surroundings at $x = d^{\mathrm{r}}$ of the right electrode, we obtain the electric potential differences across the electrode bulk phases:

$$\Delta_{\mathrm{l}}\phi = -\int_0^{d^{\mathrm{l}}} \frac{\pi(x)}{TF}\frac{\partial T}{\partial x}dx = \int_0^{d^{\mathrm{l}}} \frac{S^*_{\mathrm{e}^-}}{F}\frac{\partial T}{\partial x}dx = \frac{S^*_{\mathrm{e}^-}}{F}\Delta_{\mathrm{l}}T \tag{14}$$

$$\Delta_{\mathrm{r}}\phi = \frac{S^*_{\mathrm{e}^-}}{F}\Delta_{\mathrm{r}}T \tag{15}$$

where we assumed $S^*_{\mathrm{e}^-}$ to be constant and that the electrodes are thermostatted, i.e. $T^{\mathrm{l}} = T^{\mathrm{l,e}}$ and $T^{\mathrm{r}} = T^{\mathrm{r,e}}$. The temperature difference $\Delta_{\mathrm{l}}T = T^{\mathrm{l,e}} - T^{\mathrm{l}}_0$, see Figure 3. $\Delta_{\mathrm{r}}T$ is defined equivalently. Since $T^{\mathrm{l}}_0 = T^{\mathrm{r}}_0 = T_0$, we get the net contribution from the electrodes to the Seebeck coefficient as:

$$\frac{\Delta_{\mathrm{l}}\phi + \Delta_{\mathrm{r}}\phi}{T^{\mathrm{r,e}} - T^{\mathrm{l,e}}} = -\frac{S^*_{\mathrm{e}^-}}{F} \tag{16}$$

2.3. Electrode surfaces

The electrode reaction for the anode during battery discharge is:

$$\text{Li-}\Theta \rightarrow \text{Li}^+ + \text{e}^- + \Theta$$

where Θ is a vacancy in the host structure of the electrode. The cathode reaction is equivalent, but in the opposite direction. The entropy production of the surface is:

$$\sigma^{\text{s}} = J_q'^{\text{i}} \Delta_{\text{i,s}} \left(\frac{1}{T}\right) + J_q'^{\text{o}} \Delta_{\text{s,o}} \left(\frac{1}{T}\right) - j \frac{1}{T^{\text{s}}} \left(\Delta_{\text{i,o}}\phi + \frac{\Delta_n G^{\text{s}}}{F}\right) \tag{17}$$

Here, the rate of the chemical reaction r is uniquely coupled to the electric current density, $r = j/F$. Hence the entropy production from the electric potential jump and the Gibbs energy of the neutral components ($\Delta_n G^{\text{s}}$) combine to an effective force (see Chapter 10 in [14]). Under reversible conditions (zero entropy production), Nernst equation is recovered from the last parenthesis.

$$\left(\Delta_{\text{i,o}}\phi\right)_{j=0} = -\frac{\Delta_n G^{\text{s}}}{F} \tag{18}$$

The flux-force relations are:

$$J_q'^{\text{i}} = L^{\text{s}}_{\text{ii}} \Delta_{\text{i,s}} \frac{1}{T} + L^{\text{s}}_{\text{io}} \Delta_{\text{s,o}} \frac{1}{T} - \frac{L^{\text{s}}_{\text{i}\phi}}{T^{\text{s}}} \left(\Delta_{\text{i,o}}\phi + \frac{\Delta_n G^{\text{s}}}{F}\right) \tag{19}$$

$$J_q'^{\text{o}} = L^{\text{s}}_{\text{oi}} \Delta_{\text{i,s}} \frac{1}{T} + L^{s}_{\text{oo}} \Delta_{\text{s,o}} \frac{1}{T} - \frac{L^{\text{s}}_{\text{o}\phi}}{T^{\text{s}}} \left(\Delta_{\text{i,o}}\phi + \frac{\Delta_n G^{\text{s}}}{F}\right) \tag{20}$$

$$j = L^{\text{s}}_{\phi\text{i}} \Delta_{\text{i,s}} \frac{1}{T} + L^{\text{s}}_{\phi\text{o}} \Delta_{\text{s,o}} \frac{1}{T} - \frac{L^{\text{s}}_{\phi\phi}}{T^{\text{s}}} \left(\Delta_{\text{i,o}}\phi + \frac{\Delta_n G^{\text{s}}}{F}\right) \tag{21}$$

where again the Onsager reciprocal relations hold. The following definitions are now introduced:

$$\pi^{\text{i,o}} \equiv F \left(\frac{J_q'^{\text{i}}}{j}\right)_{\Delta_{\text{i,s}}T=0} = F \frac{L^{\text{s}}_{\text{i}\phi}}{L^{\text{s}}_{\phi\phi}} \tag{22}$$

$$\pi^{\text{o,i}} \equiv F \left(\frac{J_q'^{\text{o}}}{j}\right)_{\Delta_{\text{s,o}}T=0} = F \frac{L^{\text{s}}_{\text{o}\phi}}{L^{\text{s}}_{\phi\phi}} \tag{23}$$

$$\lambda^{\text{s,i}} \equiv \left(\frac{J_q'^{\text{i}}}{\Delta_{\text{i,s}}T}\right)_{j=0} = \frac{1}{\left(T^{\text{i,o}}\right)^2} \left(L^{\text{s}}_{\text{ii}} - \frac{\left(L^{\text{s}}_{\text{i}\phi}\right)^2}{L^{\text{s}}_{\phi\phi}}\right) \tag{24}$$

$$\lambda^{\text{s,o}} \equiv \left(\frac{J_q'^{\text{i}}}{\Delta_{\text{s,o}}T}\right)_{j=0} = \frac{1}{\left(T^{\text{o,i}}\right)^2} \left(L^{\text{s}}_{\text{oo}} - \frac{\left(L^{\text{s}}_{\text{o}\phi}\right)^2}{L^{\text{s}}_{\phi\phi}}\right) \tag{25}$$

$$r^{\text{s}} \equiv -\left(\frac{\Delta_{\text{i,o}}\phi + \frac{\Delta_n G^{\text{s}}}{F}}{j}\right)_{\Delta_{\text{i,s}}T=\Delta_{\text{s,o}}T=0} = \frac{T^{\text{s}}}{L^{\text{s}}_{\phi\phi}} \tag{26}$$

Where we assumed that coupling across the interface can be neglected, $L^{\text{s}}_{\text{io}} - \frac{L^{\text{s}}_{\text{i}\phi} L^{\text{s}}_{\phi\text{o}}}{L^{\text{s}}_{\phi\phi}} = 0$. This gives the following expressions for the thermodynamic forces at the surface:

$$\Delta_{\text{i,s}}T = -\frac{1}{\lambda^{\text{s,i}}} \left(J_q'^{\text{i}} - \frac{\pi^{\text{i}}}{F} j\right) \tag{27}$$

$$\Delta_{\text{s,o}}T = -\frac{1}{\lambda^{\text{s,o}}} \left(J_q'^{\text{o}} - \frac{\pi^{\text{o}}}{F} j\right) \tag{28}$$

$$\left(\Delta_{\mathrm{i,o}}\phi + \frac{\Delta_n G^{\mathrm{s}}}{F}\right) = -\frac{\pi^{\mathrm{i}}}{T^{\mathrm{i,o}}F}\Delta_{\mathrm{i,s}}T - \frac{\pi^{\mathrm{o}}}{T^{\mathrm{o,i}}F}\Delta_{\mathrm{s,o}}T - r^{\mathrm{s}}j \tag{29}$$

At open circuit conditions, this is further simplified. The potential jump at the left electrode surface can then be expressed as:

$$\Delta_{\mathrm{l,e}}\phi = \frac{\pi^{\mathrm{l,e}}}{T^{\mathrm{l,e}}F}(T^{\mathrm{l,e}} - T^{\mathrm{s,l}}) + \frac{\pi^{\mathrm{e,l}}}{T^{\mathrm{e,l}}F}(T^{\mathrm{s,l}} - T^{\mathrm{e,l}}) - \frac{\Delta_n G^{\mathrm{l,s}}}{F} \tag{30}$$

We assume that the jumps in temperatures at the surfaces are negligible and that $T^{\mathrm{s,r}} = T^{\mathrm{r,e}}$ and $T^{\mathrm{s,l}} = T^{\mathrm{l,e}}$. The reaction Gibbs energy, $\Delta_n G^{\mathrm{s}}$, has contributions from neutral surface components only [23], giving the contribution to the left electrode potential:

$$\frac{\Delta_n G^{\mathrm{s,l}}}{F} = \frac{1}{F}\Big(-\mu^{\mathrm{s}}_{\mathrm{Li(x,s)}}(T^{\mathrm{s,l}})\Big) \tag{31}$$

Where $\mu^{\mathrm{s}}_{\mathrm{Li(x,s)}}$ is the chemical potential of Li in the electrode surfaces. The right electrode will have the opposite sign. The partial entropy can be expressed by the following Maxwell relation:

$$S^{\mathrm{s}}_j = \left(\frac{\partial S^{\mathrm{s}}}{\partial N^{\mathrm{s}}_j}\right)_{p,T,N_{i\neq j}} = -\left(\frac{\partial \mu^{\mathrm{s}}_j}{\partial T}\right)_{p,N} \tag{32}$$

The contribution from the electrode surfaces to the Seebeck coefficient can therefore be expressed as:

$$\begin{aligned}\Delta_{\mathrm{l,e}}\phi + \Delta_{\mathrm{e,r}}\phi &= \frac{1}{F}\left(\mu^{\mathrm{s}}_{\mathrm{Li(x,s)}}(T^{\mathrm{s,l}}) - (\mu^{\mathrm{s}}_{\mathrm{Li(x,s)}}(T^{\mathrm{s,r}})\right) \\ &= \frac{1}{F}S^{\mathrm{s}}_{\mathrm{Li(x,s)}}\left(T^{\mathrm{s,r}} - T^{\mathrm{s,l}}\right)\end{aligned} \tag{33}$$

Thus

$$\left(\frac{\Delta_{\mathrm{l,e}}\phi + \Delta_{\mathrm{e,r}}\phi}{\Delta T}\right)_{j=0} = \frac{1}{F}S^{\mathrm{s}}_{\mathrm{Li(x,s)}} \tag{34}$$

This is the net contribution from both electrode interfaces to the electric potential, under the circumstances specified for the interface.

2.4. Electrolyte

The electrolyte of the cell studied here is a ternary mixture consisting of 1 M $LiPF_6$ dissolved in a 50:50 weight % of ethylene carbonate and diethyl carbonate. An application of a temperature gradient, can lead to separation of the components.

According to Prigogine [24], we can choose any frame of reference for transport in a system in mechanical equilibrium. The separator will not move compared to the laboratory frame of reference. The same is true for the electrode host-structure. They are therefore both natural frames of reference to choose. We shall nevertheless choose the DEC component as our frame of reference. The movement of this component with respect to the separator is then unknown. The advantage is that one of the chemical potentials in the electrolyte can be eliminated, using Gibbs-Duhem's equation. If we assume the separator to be inert, it will not appear as a component in the entropy production.

We will now derive expressions for the time dependence of the electric potential gradient. We can distinguish between three particular states; the initial state, with uniform composition (at time $t = 0$), the stationary state with Soret equilibrium (at time $t = \infty$), and the intermediate, quasi-stationary state (at time $t = \mathrm{int}$). At constant temperature and pressure, Gibbs-Duhem gives the following relation between the chemical potential gradients in the phase:

$$\sum_{i=1}^{3} c_i d\mu_{i,T} = 0 \tag{35}$$

where $c_i i$ is the concentration of component i and $d\mu_{i,T}$ is the change in the chemical potential at a constant temperature T. Using the Gibbs-Duhem equation the gradient of the third component can be eliminated and the entropy production

then becomes:

$$\begin{aligned}\sigma =& J'_q \frac{\partial}{\partial x}\left(\frac{1}{T}\right) - c_1\left(v_1 - v_3\right)\frac{1}{T}\left(\frac{\partial \mu_{1,T}}{\partial x}\right) \\ & - c_2\left(v_2 - v_3\right)\frac{1}{T}\left(\frac{\partial \mu_{2,T}}{\partial x}\right) - j\frac{1}{T}\left(\frac{\partial \phi}{\partial x}\right)\end{aligned} \tag{36}$$

where v_i is the velocity of component i defined by $v_i \equiv J_i/c_i$. $c_1\left(v_1 - v_3\right)$ and $c_2\left(v_2 - v_3\right)$ are then the fluxes of component 1 and 2 relative to component 3. They will be denoted as J_1 and J_2. The gradient in chemical potential for the third component disappears from the entropy production as $c_3(v_3 - v_3) = 0$. The mass fluxes are therefore not independent of each other. Because of this we need only continue with the independent fluxes, J_1 and J_2. The flux equations are then:

$$\begin{aligned}\frac{\partial}{\partial x}\left(\frac{1}{T}\right) =& r_{qq}J'_q + r_{1q}J_1 + r_{2q}J_2 + r_{q\phi}j \\ -\frac{1}{T}\left(\frac{\partial \mu_{1,T}}{\partial x}\right) =& r_{1q}J'_q + r_{11}J_1 + r_{12}J_2 + r_{1\phi}j \\ -\frac{1}{T}\left(\frac{\partial \mu_{2,T}}{\partial x}\right) =& r_{2q}J'_q + r_{21}J_1 + r_{22}J_2 + r_{2\phi}j \\ -\frac{1}{T}\left(\frac{\partial \phi}{\partial x}\right) =& r_{\phi q}J'_q + r_{\phi 1}J_1 + r_{\phi 2}J_2 + r_{\phi\phi}j\end{aligned} \tag{37}$$

where r_{ij} is the resistivity coefficients for coupling between fluxes i and j. Onsager reciprocal relations apply, so

$$\begin{aligned} r_{q1} &= r_{1q} & r_{q2} &= r_{2q} & r_{q\phi} &= r_{\phi q} \\ r_{12} &= r_{21} & r_{1\phi} &= r_{\phi 1} & r_{2\phi} &= r_{\phi 2}\end{aligned}$$

The heat flux can be found by rearranging equation 37 for the temperature gradient:

$$J'_q = -\frac{1}{r_{qq}T^2}\frac{\partial T}{\partial x} - \frac{r_{1q}}{r_{qq}}J_1 - \frac{r_{2q}}{r_{qq}}J_2 - \frac{r_{q\phi}}{r_{qq}}j \tag{38}$$

Introducing the new coefficients:

$$R_{ij} = r_{ij} - \frac{r_{iq}r_{qj}}{r_{qq}}$$

where i, j can be 1,2 or ϕ, and the following definitions:

$$q_1^* = \left(\frac{J'_q}{J_1}\right)_{dT=0,J_2=0,j=0} = -\frac{r_{q1}}{r_{qq}} \tag{39}$$

$$q_2^* = \left(\frac{J'_q}{J_2}\right)_{dT=0,J_1=0,j=0} = -\frac{r_{q2}}{r_{qq}} \tag{40}$$

$$\lambda = \left(\frac{J'_q}{\partial T/\partial x}\right)_{j=0,J_1=J_2=0} = \frac{1}{r_{qq}T^2} \tag{41}$$

where q_i^* is the heat of transfer of component i. The flux-force relations are now:

$$\begin{aligned}J'_q &= -\lambda\frac{\partial T}{\partial x} + q_1^*J_1 + q_2^*J_2 - \frac{r_{q\phi}}{r_{qq}}j \\ -\frac{1}{T}\frac{\partial \mu_{1,T}}{\partial x} &= \frac{q_1^*}{T^2}\frac{\partial T}{\partial x} + R_{11}J_1 + R_{12}J_2 + R_{1\phi}j \\ -\frac{1}{T}\frac{\partial \mu_{2,T}}{\partial x} &= \frac{q_2^*}{T^2}\frac{\partial T}{\partial x} + R_{21}J_1 + R_{22}J_2 + R_{2\phi}j \\ -\frac{1}{T}\left(\frac{\partial \phi}{\partial x}\right) &= -\frac{r_{\phi q}}{r_{qq}T^2}\frac{\partial T}{\partial x} + R_{\phi 1}J_1 + R_{\phi 2}J_2 + R_{\phi\phi}j\end{aligned} \tag{42}$$

Solving for the mass fluxes

$$\begin{aligned} J_1 = &- \frac{L_{11}}{T}\left(\frac{\partial \mu_{1,T}}{\partial x} + \frac{q_1^*}{T}\frac{\partial T}{\partial x}\right) - \frac{L_{12}}{T}\left(\frac{\partial \mu_{2,T}}{\partial x} + \frac{q_2^*}{T}\frac{\partial T}{\partial x}\right) \\ &- \left(R_{1\phi}L_{11} + R_{2\phi}L_{12}\right) j \\ J_2 = &- \frac{L_{12}}{T}\left(\frac{\partial \mu_{1,T}}{\partial x} + \frac{q_1^*}{T}\frac{\partial T}{\partial x}\right) - \frac{L_{22}}{T}\left(\frac{\partial \mu_{2,T}}{\partial x} + \frac{q_2^*}{T}\frac{\partial T}{\partial x}\right) \\ &- \left(R_{1\phi}L_{12} + R_{2\phi}L_{22}\right) j \end{aligned} \tag{43}$$

where

$$L_{11} = \frac{R_{22}}{R_{11}R_{22} - R_{12}R_{21}} \qquad L_{22} = \frac{R_{11}}{R_{11}R_{22} - R_{12}R_{21}}$$
$$L_{12} = L_{21} = -\frac{R_{12}}{R_{11}R_{22} - R_{12}R_{21}}$$

and

$$R_{11} = \frac{L_{22}}{L_{11}L_{22} - L_{12}L_{21}} \qquad R_{22} = \frac{L_{11}}{L_{11}L_{22} - L_{12}L_{21}}$$
$$R_{12} = R_{21} = -\frac{L_{12}}{L_{11}L_{22} - L_{12}L_{21}}$$

We can rewrite the chemical potential gradients as:

$$\frac{\partial \mu_{i,T}}{\partial x} = \sum_j \Gamma_{ij}\frac{RT}{c_j}\frac{\partial c_j}{\partial x} \tag{44}$$

where Γ_{ij} is the thermodynamic factor:

$$\Gamma_{ij} = \left(\frac{\partial \mu_{i,T}}{\partial c_j}\right)_{c_{i\neq j}} \frac{c_j}{RT} \tag{45}$$

Since the chemical potential gradients are related through Gibbs-Duhem (see Eq. 35), we can show that the two independent terms can be expressed as a linear combination of $\partial c_1/\partial x$ and $\partial c_2/\partial x$:

$$\begin{aligned} \frac{\partial \mu_{1,T}}{\partial x} &= a_{11}\frac{\partial c_1}{\partial x} + a_{12}\frac{\partial c_2}{\partial x} \\ \frac{\partial \mu_{2,T}}{\partial x} &= a_{21}\frac{\partial c_1}{\partial x} + a_{22}\frac{\partial c_2}{\partial x} \end{aligned} \tag{46}$$

The full expression for a_{ij} is given in the Appendix.

$$\begin{aligned} J_1 = &- \frac{L_{11}}{T}\left(a_{11}\frac{\partial c_1}{\partial x} + a_{12}\frac{\partial c_2}{\partial x} + \frac{q_1^*}{T}\frac{\partial T}{\partial x}\right) \\ &- \frac{L_{12}}{T}\left(a_{21}\frac{\partial c_1}{\partial x} + a_{22}\frac{\partial c_2}{\partial x} + \frac{q_2^*}{T}\frac{\partial T}{\partial x}\right) \\ &- \left(R_{1\phi}L_{11} + R_{2\phi}L_{12}\right) j \\ J_2 = &- \frac{L_{12}}{T}\left(a_{11}\frac{\partial c_1}{\partial x} + a_{12}\frac{\partial c_2}{\partial x} + \frac{q_1^*}{T}\frac{\partial T}{\partial x}\right) \\ &- \frac{L_{22}}{T}\left(a_{21}\frac{\partial c_1}{\partial x} + a_{22}\frac{\partial c_2}{\partial x} + \frac{q_2^*}{T}\frac{\partial T}{\partial x}\right) \\ &- \left(R_{1\phi}L_{12} + R_{2\phi}L_{22}\right) j \end{aligned} \tag{47}$$

We can now define the transfer coefficients (t_i), transported entropy of Li^+ and the Peltier coefficient for the electrolyte:

$$\begin{aligned}
t_1 &= \left(\frac{J_1}{j/F}\right)_{dT=0,d\mu_{1,T}=d\mu_{2,T}=0} = \left(\frac{F\partial\phi/\partial x}{\partial\mu_{1,T}/\partial x}\right)_{dT=0,j=0} \\
&= -F\left(R_{1\phi}L_{11} + R_{2\phi}L_{12}\right) \\
t_2 &= \left(\frac{J_2}{j/F}\right)_{dT=0,d\mu_{1,T}=d\mu_{2,T}=0} = \left(\frac{F\partial\phi/\partial x}{\partial\mu_{2,T}/\partial x}\right)_{dT=0,j=0} \\
&= -F\left(R_{1\phi}L_{12} + R_{2\phi}L_{22}\right) \\
S^*_{Li^+} &= -F\frac{r_{q\phi}}{r_{qq}T} \\
\pi &= \left(\frac{J'_q}{j/F}\right)_{dT=0,d\mu_{1,T}=d\mu_{2,T}=0} = -FT\left(\frac{\partial\phi/\partial x}{\partial T/\partial x}\right)_{dc_1=dc_2=0,j=0} \\
&= t_1q^*_1 + t_2q^*_2 + TS^*_{Li^+}
\end{aligned} \tag{48}$$

and the diffusion coefficients (D_{ij}), thermal diffusion coefficients ($D_{i,T}$) and ohmic resistivity:

$$\begin{aligned}
D_{11} &= -\left(\frac{J_1}{\partial c_1/\partial x}\right)_{dT=0,dc_2=0,j=0} = \frac{1}{T}\left(L_{11}a_{11} + L_{12}a_{21}\right) \\
D_{12} &= -\left(\frac{J_1}{\partial c_2/\partial x}\right)_{dT=0,dc_1=0,j=0} = \frac{1}{T}\left(L_{11}a_{12} + L_{12}a_{22}\right) \\
D_{21} &= -\left(\frac{J_2}{\partial c_1/\partial x}\right)_{dT=0,dc_2=0,j=0} = \frac{1}{T}\left(L_{12}a_{11} + L_{22}a_{21}\right) \\
D_{22} &= -\left(\frac{J_2}{\partial c_2/\partial x}\right)_{dT=0,dc_1=0,j=0} = \frac{1}{T}\left(L_{12}a_{12} + L_{22}a_{22}\right) \\
D_{1T} &= -\left(\frac{J_1}{c_1\partial T/\partial x}\right)_{dc_1=dc_2=0,j=0} = \frac{L_{11}q^*_1 + L_{12}q^*_2}{c_1T^2} \\
D_{2T} &= -\left(\frac{J_2}{c_2\partial T/\partial x}\right)_{dc_1=dc_2=0,j=0} = \frac{L_{12}q^*_1 + L_{22}q^*_2}{c_2T^2} \\
r &= -\left(\frac{\partial\phi/\partial x}{j}\right)_{dT=0,dc_1=dc_2=0} = T\left(R_{1\phi}\frac{t_1}{F} + R_{2\phi}\frac{t_2}{F} - R_{\phi\phi}\right) \\
&= -T\left(R^2_{1\phi}L_{11} + 2R_{1\phi}R_{2\phi}L_{12} + R^2_{2\phi}L_{22} + R_{\phi\phi}\right)
\end{aligned} \tag{49}$$

Note that the matrix of diffusion coefficients is not symmetric. The flux-force relations can be written:

$$\begin{aligned}
J'_q &= -\lambda\frac{\partial T}{\partial x} + q^*_1\left(J_1 - \frac{t_1}{F}j\right) + q^*_2\left(J_2 - \frac{t_2}{F}j\right) + \frac{\pi}{F}j \\
J_1 &= -D_{11}\frac{\partial c_1}{\partial x} - D_{12}\frac{\partial c_2}{\partial x} - c_1D_{1T}\frac{\partial T}{\partial x} + \frac{t_1}{F}j \\
J_2 &= -D_{21}\frac{\partial c_1}{\partial x} - D_{22}\frac{\partial c_2}{\partial x} - c_2D_{2T}\frac{\partial T}{\partial x} + \frac{t_2}{F}j \\
F\frac{\partial\phi}{\partial x} &= -\frac{\pi}{T}\frac{\partial T}{\partial x} - \left(t_1a_{11} + t_2a_{21}\right)\frac{\partial c_1}{\partial x} \\
&\quad - \left(t_1a_{12} + t_2a_{22}\right)\frac{\partial c_2}{\partial x} - Frj
\end{aligned} \tag{50}$$

To simplify notation we introduce:

$$\begin{aligned}
b_1 &= \left(t_1a_{11} + t_2a_{21}\right) \\
b_2 &= \left(t_1a_{12} + t_2a_{22}\right)
\end{aligned}$$

We have

$$q_1^* = \left(\frac{J_q'}{J_1}\right)_{\Delta T=0,J_{2,}=0,j=0} = -T\left(\frac{\partial \mu_{1,T}/\partial x}{\partial T/\partial x}\right)_{j=0,J_1=J_2=0} \tag{51}$$

and equivalently for q_2^*, so when the concentration gradients are fully developed, the terms containing heats of transfer in the Peltier coefficient are cancelled against the concentration gradient terms. By integrating across the thickness of the electrolyte, we find the electric potential difference across the electrolyte at open circuit conditions:

$$\begin{aligned} F\Delta_{\mathrm{e}}\phi =& F\int_{d^{\mathrm{l}}}^{d^{\mathrm{e}}} \frac{\partial \phi}{\partial x} dx = -S^*_{\mathrm{Li}^+}\Delta_{\mathrm{e}}T \\ & - t_1 q_1^{*,\mathrm{e}} \ln\left(\frac{T(d^{\mathrm{e}})}{T(d^{\mathrm{l}})}\right) - t_2 q_2^{*,\mathrm{e}} \ln\left(\frac{T(d^{\mathrm{e}})}{T(d^{\mathrm{l}})}\right) \\ & - b_1\Delta_{\mathrm{e}}c_1 - b_2\Delta_{\mathrm{e}}c_2 \end{aligned} \tag{52}$$

$\Delta_{\mathrm{e}}c_1$ and $\Delta_{\mathrm{e}}c_2$ will vary with time as concentration gradients build up due to the thermal driving force. Using that $\Delta_{\mathrm{e}}T \ll T(d^{\mathrm{l}})$ the contribution to the thermoelectric potential of the electrolyte becomes

$$\begin{aligned} \frac{\Delta_{\mathrm{e}}\phi}{\Delta_{\mathrm{e}}T} =& -\frac{S^*_{\mathrm{Li}^+}}{F} - \frac{t_1 q_1^*}{TF} - \frac{t_2 q_2^*}{TF} - \frac{1}{F} b_1 \frac{\Delta_{\mathrm{e}}c_1}{\Delta_{\mathrm{e}}T} \\ & - \frac{1}{F} b_2 \frac{\Delta_{\mathrm{e}}c_2}{\Delta_{\mathrm{e}}T} \end{aligned} \tag{53}$$

Unlike the other contributions, this depends on time, as there is a time evolution of the concentration difference, towards a stationary value. We shall specify this contribution below.

2.5. The time-dependent Seebeck coefficient

We are now in position to add all contributions to the total potential. Because we have thermostatted electrodes, the temperature differences are the same in equation 16, 34 and 53, i.e. the difference in temperature between the two electrode surfaces. In other words, the temperature difference is across the electrolyte. We add Eqs.16 and 34 to Eq. 53, and obtain a general formula for the time dependent Seebeck coefficient:

$$\begin{aligned} \epsilon_t \equiv \left(\frac{\Delta_{\mathrm{tot}}\phi}{\Delta T}\right)_{j=0} =& \frac{1}{F}\left(S_{\mathrm{Li}} - S^*_{\mathrm{e}^-} - S^*_{\mathrm{Li}^+} - \frac{t_1 q_1^*}{T} - \frac{t_2 q_2^*}{T}\right) \\ & - \frac{1}{F}\left(b_1 \frac{\Delta c_1}{\Delta_T} + b_2 \frac{\Delta c_2}{\Delta T}\right) \end{aligned} \tag{54}$$

Here ΔT is the temperature difference between the left and right electrodes. Subscript t indicates that the ratio is time-dependent. The time-dependence is not explicit in this expression. An explicit expression can be found in the present case. There are two time-dependent diffusional processes. In the present case they happen on widely separated time scales. We shall see, that the first is equilibrated within hours, while the second takes days to reach stationary state. Bierlein [25] gave a solution for Δc_i for small deviations in the equilibrium concentration, negligible changes in the density with composition, at constant ΔT:

$$\Delta c_i = s_{T,i}\Delta T c_{0,i}\left(1 - c_{0,i}/c_{\mathrm{tot}}\right)\left[1 - \frac{8}{\pi^2}\exp\left(-t/\theta_i\right)\right] \tag{55}$$

where c_i/c_{tot} is the molar fraction, $s_{T,i}$ is the Soret coefficient of component i and π is the constant. In the absence of coupling between the diffusional fluxes (the diffusion processes take place on separated time scales), we can write Soret coefficients as for binary systems, as the ratio of the thermal and the normal diffusion coefficient, $s_{T,i} = D_{T,i}/D_{ii}$. De Groot defined the relaxation time θ_i [22]:

$$\theta_i = \frac{(\tau h)^2}{\pi^2 D_{ii}} \tag{56}$$

where h is the distance between the electrodes. In a liquid electrolyte, h would be the distance between the two electrodes, and τ is the tortuosity of the porous medium. This property is not far from unity in the separator used here, which has very big pores. The diffusion coefficient in the pores is thus related to the bulk diffusion coefficient by $D_{ii} = D_{ii}^{\text{eff}}\tau^2$ [26]. Equation 55 applies when $t > \theta_i/3$ [27].

Component 1 will reach Soret equilibrium first, at ϵ_{int}. For the first Soret equilibrium we then have [27]:

$$\begin{aligned}\epsilon_t =& \epsilon_0 - \frac{1}{F} b_1 \frac{D_{1T}}{D_{11}} c_{1,0} \left(1 - \frac{c_{1,0}}{c_{\text{tot}}}\right)\left[1 - \frac{8}{\pi^2}\exp\left(-t/\theta_1\right)\right] \\ =& \epsilon_{\text{int}} - \left(\epsilon_{\text{int}} - \epsilon_0\right)\frac{8}{\pi^2}\exp\left(-t/\theta_1\right)\end{aligned} \tag{57}$$

Component 2 approaches full Soret equilibrium after this. The starting composition c_0 of the second process is the final composition of the completed first process.

$$\begin{aligned}\epsilon_t =& \epsilon_0' - \frac{1}{F} b_2 \frac{D_{T,2}}{D_{22}} c_{2,0} \left(1 - \frac{c_{2,0}}{c_{\text{tot}}}\right)\left[1 - \frac{8}{\pi^2}\exp\left(-t/\theta_2\right)\right] \\ =& \epsilon_\infty - \left(\epsilon_\infty - \epsilon_{\text{int}}\right)\frac{8}{\pi^2}\exp\left(-t/\theta_2\right)\end{aligned} \tag{58}$$

3. Theory Summary

In the preceding section, we computed the various contributions to the cell's Seebeck coefficient, and found the time-dependence of the total potential difference under certain assumptions. The conditions applied to cells, with 100 % Li-intercalated electrodes and two separable time-dependent diffusional processes. Here we repeat the essential expressions, to be used for the data reduction in the next section.

The expression that applies at initial times (no concentration gradients, uniform ternary electrolyte) is:

$$\epsilon_0 \equiv \left(\frac{\Delta\phi}{\Delta T}\right)_{j=0,t=0} = \frac{1}{F}\left(-S^*_{\text{e}^-} + S_{\text{Li}} - S^*_{\text{Li}^+} - \frac{t_1 q_1^*}{T} - \frac{t_2 q_2^*}{T}\right) \tag{59}$$

The expression that applies at partial Soret equilibrium, when the first concentration gradient is established, is:

$$\epsilon_{\text{int}} \equiv \left(\frac{\Delta\phi}{\Delta T}\right)_{j=0,t=\text{int}} = \frac{1}{F}\left(-S^*_{\text{e}^-} + S_{\text{Li}} - S^*_{\text{Li}^+} - \frac{t_2 q_2^*}{T}\right) \tag{60}$$

The expression that applies at full Soret equilibrium (final stationary state), when the $\Delta c/\Delta T$ terms cancel the heat of transfer terms, is:

$$\epsilon_\infty \equiv \left(\frac{\Delta\phi}{\Delta T}\right)_{j=0,t=\infty} = \frac{1}{F}\left(-S^*_{\text{e}^-} + S_{\text{Li}} - S^*_{\text{Li}^+}\right) \tag{61}$$

We see from the last expression, that knowledge of the lithium entropy in the electrodes, will allow us to compute the transported entropy of lithium in the electrolyte. Once this is known, we can find each of the terms containing a heat of transfer and a transport number. Information on transport numbers are needed to further decompose these terms.

The general expression for the Seebeck coefficient as a function of time is

$$\begin{aligned}\epsilon_t \equiv& \left(\frac{\Delta_{\text{tot}}\phi}{\Delta T}\right)_{j=0} \\ =& \frac{1}{F}\left(S_{\text{Li}} - S^*_{\text{e}^-} - S^*_{\text{Li}^+} - \frac{t_1 q_1^*}{T} - \frac{t_2 q_2^*}{T}\right) \\ & - \frac{1}{F}\left(b_1\frac{\Delta c_1}{\Delta T} + b_2\frac{\Delta c_2}{\Delta T}\right) \\ =& \epsilon_0 - \frac{1}{F} b_1 \frac{D_{T,1}}{D_{11}} c_{0,1}\left(1 - c_{0,1}/c_{\text{tot}}\right)\left[1 - \frac{8}{\pi^2}\exp\left(-t/\theta_1\right)\right] \\ & - \frac{1}{F} b_2 \frac{D_{T,2}}{D_{22}} c_{0,2}\left(1 - c_{0,2}/c_{\text{tot}}\right)\left[1 - \frac{8}{\pi^2}\exp\left(-t/\theta_2\right)\right]\end{aligned} \tag{62}$$

In Eqs. 57 and 58 this has been divided into two processes, which are expressed terms of the initial, intermediate and final values for the Seebeck coefficent (see [27]). This time evolution of ϵ_t gives θ_i and D_{ii}^{eff} from curve-fits to exponential functions. Information of the Seebeck coefficient, of the partial Soret equilibrium could also extracted from these curves.

We can now see that the composition-dependent Peltier heat is given by (see Eq. 3):

$$\begin{aligned}\pi = &- T\left(S_{\text{Li}} - S^*_{\text{e}^-} - S^*_{\text{Li}^+} - t_1 q_1^* - t_2 q_2^*\right) \\ &+ T\left(b_1 \frac{\Delta c_1}{\Delta T} + b_2 \frac{\Delta c_2}{\Delta T}\right)\end{aligned} \tag{63}$$

Now the detrimental mistake done in literature becomes clear. It is not possible to find the local heat effects by splitting $T\Delta S$ into an entropy changes from the anode and cathode alone, commonly referred to as half-cell entropies. Transported entropies and heats cannot be neglected. Equation 1 applies, but the Peltier heats are complicated, as shown by Eq. 63. We have seen before that the Peltier heat can be substantial [18].

4. Experimental

Thermoelectric cells were constructed in order to find the local heat sources and sinks as described in the theory. We describe first the assembly of pouch cells and the calibration of the thermocouples. The experimental set-up for potential measurements and the experimental procedure are described next.

4.1. Pouch cell assembly and thermocouple calibration

The pouch cell housing material consisted of a laminate of 12 µm polyester polyethylene terephtalate (PET), 9 µm aluminium and 100 µm polyethylene (PE). The laminate was cut to 4 cm height and 4 cm width. We consider these dimensions sufficient to ensure one-dimensional transport between the electrodes. The PE layer of the laminate melts by moderate heating, and this was used to seal the cell. As connector material to the electrodes, we used aluminium. The $LiFePO_4$ electrodes were type HS-LIB-P-LFP-001 from Hohsen.

The assembly of the pouch cells is illustrated in Figure 5.

Electrodes and separators, Whatman Glass Microfibre Filters GF/D (no 1823070, pore diameter of 2.7 µm), were stacked inside the pouch. The total thickness of the electrolyte soaked separator stack was 1.8 mm. The thickness was chosen to ensure that the temperature gradient was established across the electrolyte, between the electrodes (see Eq. 54). The bonding film (3M, article number TBF615), used to seal the side with the current collectors, was held in place with tape, article number SC-100-10 from 3M.

The electrolyte was the LP40 electrolyte from BASF consisting of a 1 M solution of $LiPF_6$ and a 50:50 mixture of EC/DEC by weight. The component concentrations were 0.528 mol/kg, 5.223 mol/kg and 3.893 mol/kg for $LiPF_6$, EC and DEC, respectively. The mole fractions were then x_1=0.0547, x_2=0.5416 and x_3=0.4037.

Electrolyte was added drop-wise to the separator stack inside a glove-box. The pouch was put under vacuum before the final side was sealed by applying heat. The cell was put in a frame that held the parts together. Water was circulating in aluminum plates on the top and bottom, see Figure 6. A temperature difference was established using two water baths (Grant Lt ecocool 100). The hot water flow was positioned on the top of the cell to avoid convection in the electrolyte. The aluminium plates for water circulation were in contact with copper plates. This ensured a constant temperature difference between the hot and cold sides of the pouch cell. The external temperature difference, ΔT_0, was measured between the copper plates using K-type precision fine wire thermocouples from Omega. The temperature difference was measured within ±0.01 K. The average temperature was kept constant at 25.0±0.1°C throughout the experiments. The water baths were set to give water bath temperature differences of 5, 10, 12.5, and 20°C.

In order to find the temperature difference between the electrodes inside the thermocell, ΔT, we calibrated the symmetric $LiCoO_2$ cell as described earlier [18]. In five experiments, the ratio of the electrode temperature difference and the bath temperature difference was determined to $\Delta T/\Delta T_0 = 0.70 \pm 0.01$. Our cell resemble this cell in the cell dimensions and materials' thermal conductivities [18, 28, 29], so we adopt these calibration results.

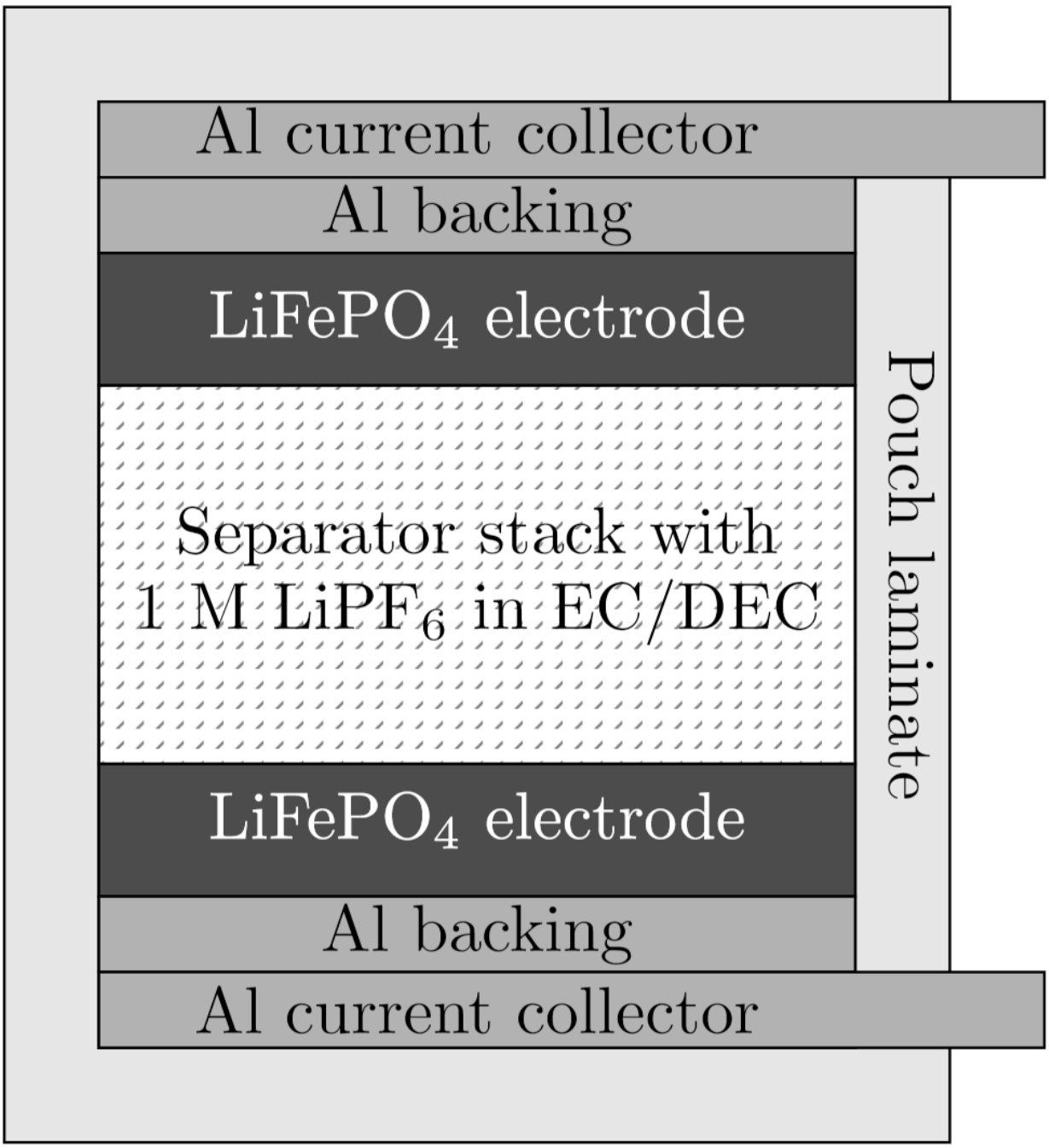

Figure 5: Components of a pouch cell schematically.

4.2. Emf Measurements

The experimental set up is illustrated in Figure 6. The electric potential was recorded using an Agilent 34970A Data acquisition/Switch unit. Prior to the measurements, the cells were short-circuited for 3 days and allowed to equilibriate until a stationary bias potential was reached. Ideally the bias potential should be zero. In practice the electrodes differed by a few mV, before a temperature difference was applied. Cells with higher bias potential were not

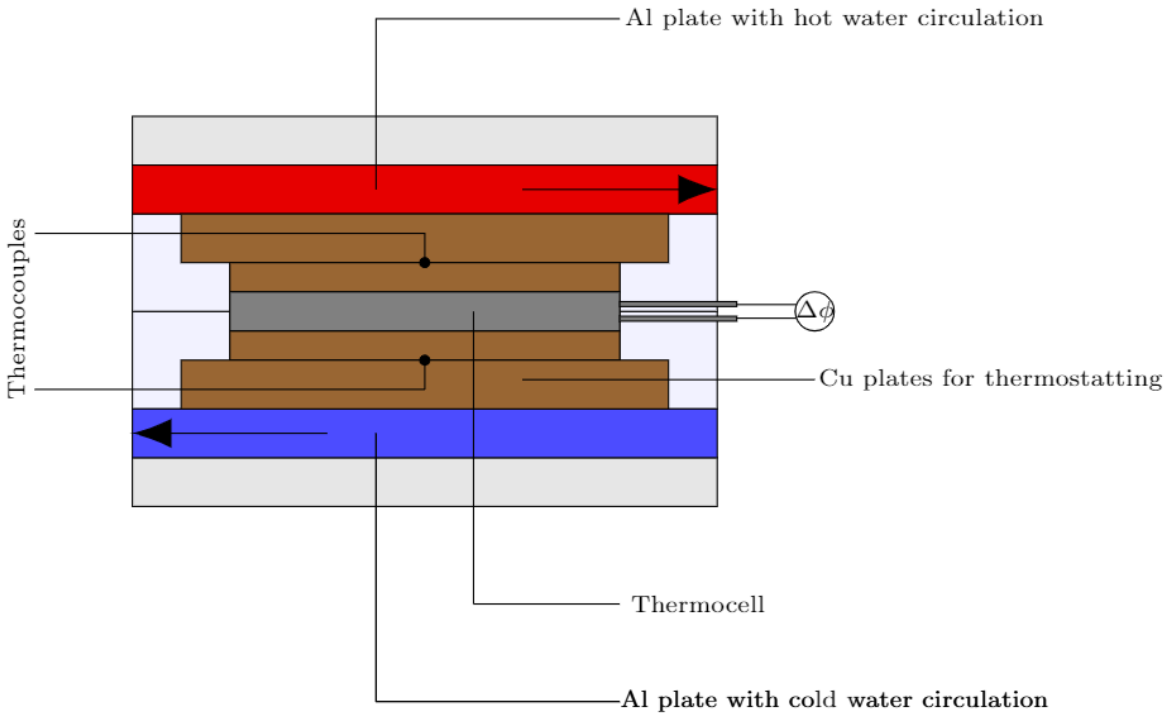

Figure 6: Schematic diagram of the experimental set up. The temperature difference was set by circulating water from water baths. The thermocell was thermostatted by sandwiching the cell between copper plates. The temperature was measured between two copper plates on both sides of the cell. The current collectors of the thermocell were connected to a multimeter.

trusted, but gave the same steady state values. The potential was measured before, during and after the temperature difference was applied. The electric potential was recorded as a function of time until the stationary state(s) were reached, and again after equilibrium was reached, once the temperature difference was removed. This typically took 7 days with the cells made for these measurements.

5. Results and Discussion

The results are presented in Figures 7 -10 and Tables 1-5. All results apply to a cell with two $LiFePO_4$ electrodes.

The time-variation in the electric potential is first presented, see Figures 7-8. From analyses of these figures, we determined the Seebeck coefficients of the initial, intermediate and final stationary states, see Tables 1-4, and we derived characteristic times for interdiffusion of two components in a thermal gradient, along with the components' main effective diffusion coefficients (Table 1).

The Seebeck coefficients enabled us to compute the Peltier heats under various conditions; *i.e.* the heat sinks and sources at the electrodes in the various stationary states. The Peltier heats will be needed for a complete thermal model of the battery. The results are discussed as they are presented.

5.1. Time-evolution of the thermoelectric potential

The typical time-evolution of the temperature and the corresponding cell potential is shown in Figure 7 and, as a close-up, in Figure 8. The upper (red) curves in both figures show the temperature difference between the two water baths as a function of time. Some fifteen minutes were needed to change from isothermal conditions to a stable temperature difference between the baths. The first figure represents a bath temperature differences of 12.5 K.

The variation in the electric potential from the start of the experiment ($t = 0$) until the (final) stationary state at $t = \infty$, is shown in the lower part of the figure. During the initial increase in the temperature difference to a constant level (top curve Figure 7), the corresponding electric potential first decreased, before it passed through a local minimum, followed by a slow decrease to a stationary plateau value ($t = \infty$). The local minimum, reached after about 60 minutes after the temperature difference was applied, is best seen from the close-up in Figure 8.

We can thus speak of an initial (within 15 minutes), an intermediate (local minimum in the response), and a stationary state ($t = \infty$), corresponding to the start -, the minimum -, and the final plateau value. The signal returns to a base-line, as expected, when ΔT is removed. The return is via a local minimum after about 60 minutes. Results for water bath temperature differences of 5, 10, 12.5 and 20 K were obtained. The results pictured were obtained for water bath temperature difference $\Delta T = 12.5$ K. From now on the experiments will be described by the internal ΔT, which was 2.4, 4.7, 5.7, 6.9 and 9.2 K.

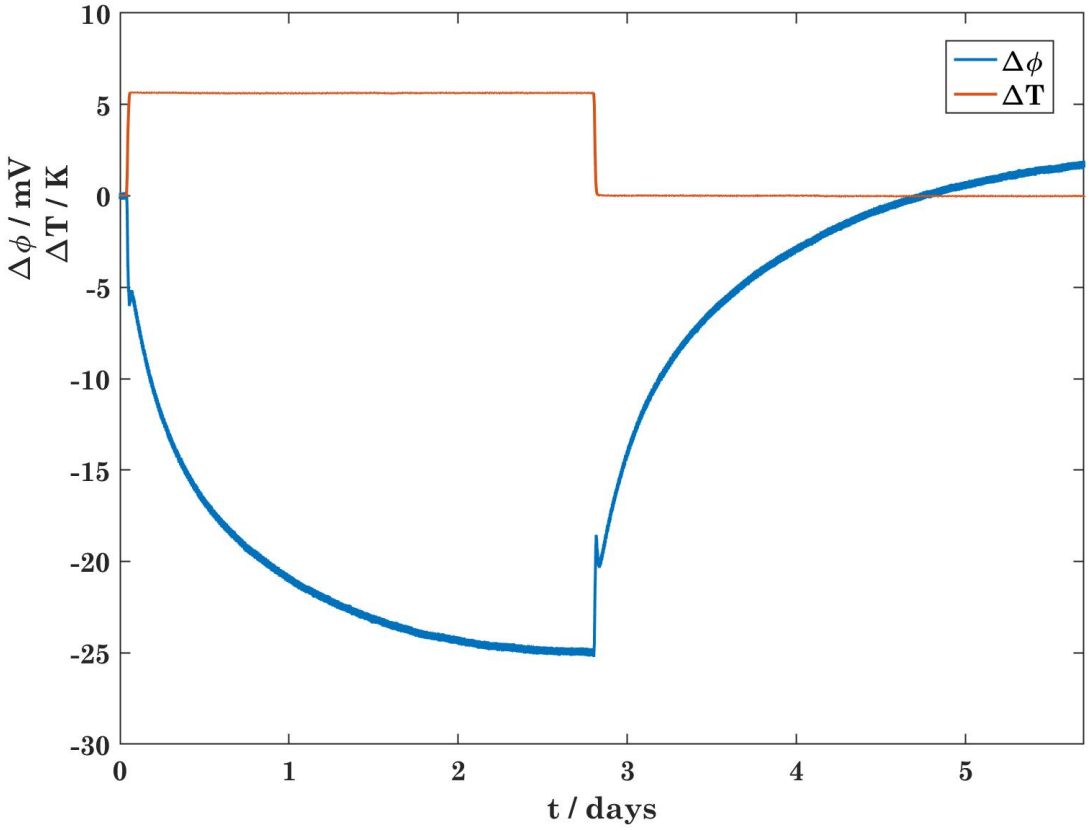

Figure 7: The temperature difference and the electric potential of the $LiFePO_4$ symmetric cell as a function of time.

5.1.1. Two time-dependent phenomena in the electrolyte

The initial phase of the response (at times less than 15 minutes), when the temperature difference is established, can be explained by the cell's response to a change in thermal boundary conditions. This phase is not of direct interest.

The changes on the longer time-scales give the information that we are seeking. The results indicate that there are two time-dependent processes. The existence of a local minimum around 60 minutes with a further rise and decline to a stationary value, can only be explained by the existence of two time-dependent processes that counteract each other,

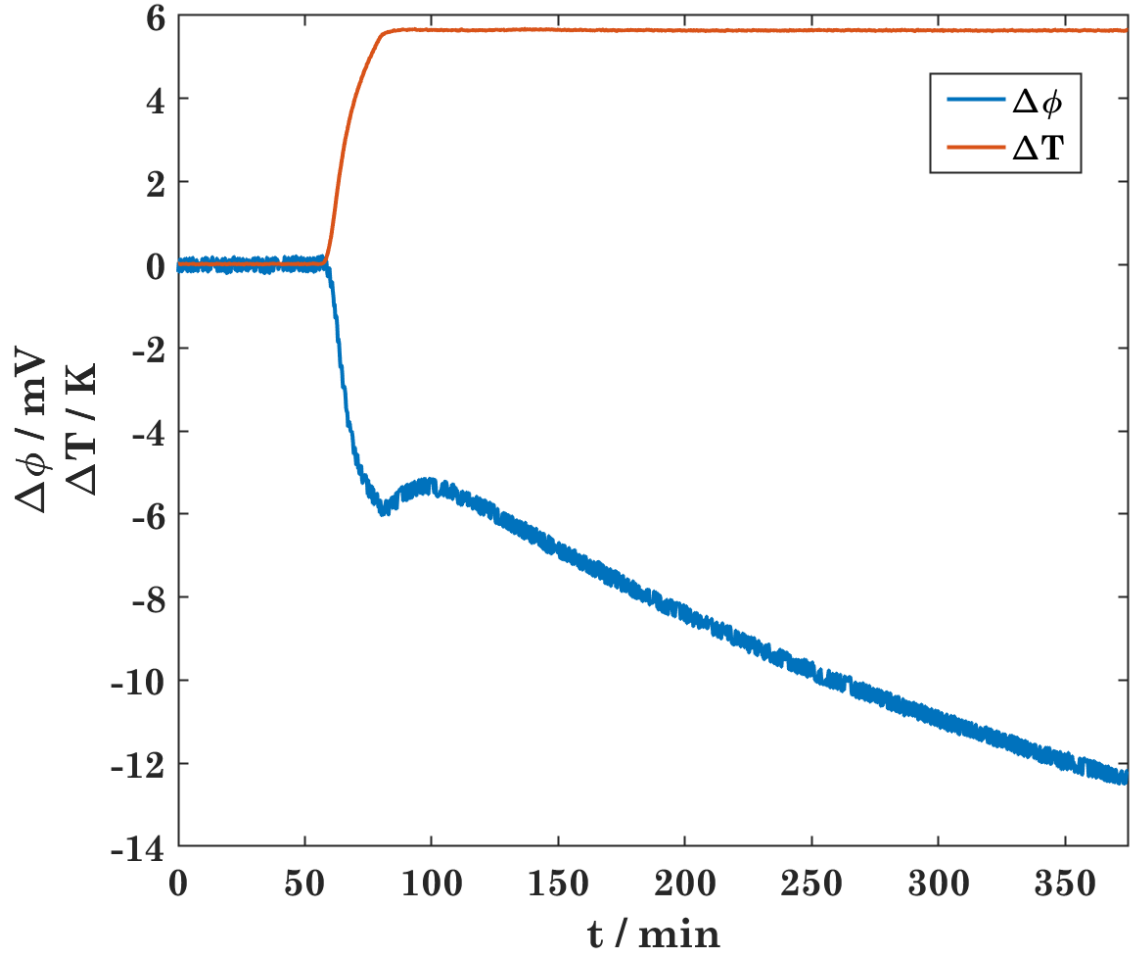

Figure 8: A zoom-in of the electric potential in Figure 7 for the start of the experiment. The electrodes were of $LiFePO_4$ and the water bath temperature difference was set to 12.5 K.

having opposite effects on the potential. While the first process leads to a decrease in the (negative) electric potential, the second leads to an increase.

This interpretation is supported by the behavior that we observe after removing the temperature difference. We then see a slow return of the electric signal back to the base-line. Superimposed on a slow process, there is a faster event, leading to a local minimum.

The signal does not return to zero (as expected) calling for corrections by drift in the signal, but the overall process is also now composed of a fast and a slow equilibration step.

This behavior of the electric potential has support in the theory given above. The temperature gradient acts as a force also on the mass fluxes. A mass fluxes will build a concentration gradient across the cell through thermal diffusion. The various components in the electrolyte have different relaxation times, one much faster than the other. Therefore, we see the development of an intermediate stationary state, where the first component is at quasi-equilibrium in the thermal field, before a balance of forces or Soret equilibrium is reached in the end for the slow component. During the last process the first may readjust somewhat.

It is reasonable to choose the largest molecule (DEC) as a frame of reference for the diffusion processes. DEC may move relative to the walls, but this does not affect the argument; there are only two independent diffusional processes.

The lithium hexafluoro-phosphate and the ethylene carbonate (EC) will move relative to DEC in a temperature gradient. We next find it reasonable to allocate the faster of the two diffusion processes to the lithium salt. The approach to the first local minimum can then be understood as a first attempt to reach a partial Soret equilibrium for the salt in an (average) carbonate-solvent. In the much slower step, the two carbonate compounds will (be forced to) separate and create a gradient of diethyl carbonate in ethylene carbonate. The hexafluorophosphate may readjust itself in this process. Further work is needed to confirm which Soret equilibrium can be contributed to which component. For now we assume that the first peak is caused by the lithium salt.

5.2. Seebeck coefficient determinations at initial, intermediate and infinite times

For each temperature difference, the observed time-variation of the electric potential was decomposed according to formulae 57-58 in the Theory section to give the potential differences corresponding to initial ($\epsilon_{t=0}$), intermediate ($\epsilon_{t=\text{int}}$) and final stationary state Seebeck coefficients ($\epsilon_{t=\infty}$). The following procedure was used:

- The stationary state Seebeck coefficient ($\epsilon_{t=\infty}$) was first determined, by plotting $\Delta\phi$, the final state value, vs ΔT. An example of such a plot is shown in Figure 9. The Seebeck coefficient is the slope of the plot, giving -3.7 ± 0.8 mV/K in this case.
- Using knowledge of $\epsilon_{t=\infty}$, we next extracted ϵ_{int} by fitting experimental data from the tail of the experiment to the first part of the relaxation curve, see Figure 10 lower part.
- The initial value, $\epsilon_{t=0}$, was next derived. We used the difference between the end stationary state and the local peak following the removal of the temperature difference to derive $\epsilon_{t=0}$. The response of the electrodes to removal of the temperature difference was more immediate than the response to application of a temperature difference, and gave a more precise fit. The rapid response can be seen in Figure 7.
- The exponents of the fits to the relaxation curves gave the characteristic diffusion times (θ_1, θ_2) and the diffusion coefficients (D_1, D_2).

The bias potential of Figure 9, can be read as an intercept with the ordinate axis, here 3.2 mV. In general, the bias potential varied over the time course of the experiment by ±0.5 − 2 mV. The drift had little impact on the Seebeck coefficients, however. All resulting Seebeck coefficients are given in Table 2. The same average value observed at infinite times were also observed for cells with a higher bias potential (not shown). The initial Seebeck coefficient, ϵ_0, was also confirmed by extrapolating curves like the one given in Figure 9 to $t = 0$. The results were less precise, but within the uncertainty of the measurements and supported the values from the fits.

The value of $\epsilon_{t=\infty}$ did not depend significantly on the magnitude of the temperature difference, as shown in Table 2. The average stationary state thermoelectric potential was -4.3 ± 0.6 mV/K, see Table 2.

We have seen above that two diffusional phenomena are present in the electrolyte, but also that they are widely separated on different time scales. The approximations behind the expression of Bierlein et al. [25] are therefore valid, and we have probably a good estimate of the characteristic times and the corresponding effective diffusion coefficients of the components in question. The experimental data in Table 2 were used with Eqs. 57 and 58. An example of the fit for the experiment with $\Delta T = 2.4$ is shown in Figure 10, resulting in:

$$\epsilon_t \approx \begin{cases} -0.9 - (-1.3 - (-0.9)) \cdot \exp\left(-0.1 \cdot t\right)\Big) & t < 40\text{min} \\ -4.5 - (-4.5 - (-0.9)) \cdot \exp\left(-0.0011 \cdot t\right)\Big) & t > 300\text{min} \end{cases}$$

The fit was made for the electric potential divided by the average ΔT. For the fit approaching the first Soret coefficient the average initial and intermediate values were used, while the $\Delta T = 2.4$ measurement was used for ϵ_∞. This was due to the larger relative uncertainty in the two first values. The coefficients in front of the exponential and the constants were then used as in Eqs. 57-58. The relaxation time was then found by fitting it to the experimental curve. The fitted curves are shown in Figure 10. We observed that the fit, or the agreement with theory was better at large times, i.e. $t > \theta/3$. This is in agreement with the theory we use [27]. Similar curves can be used to describe all the experiments.

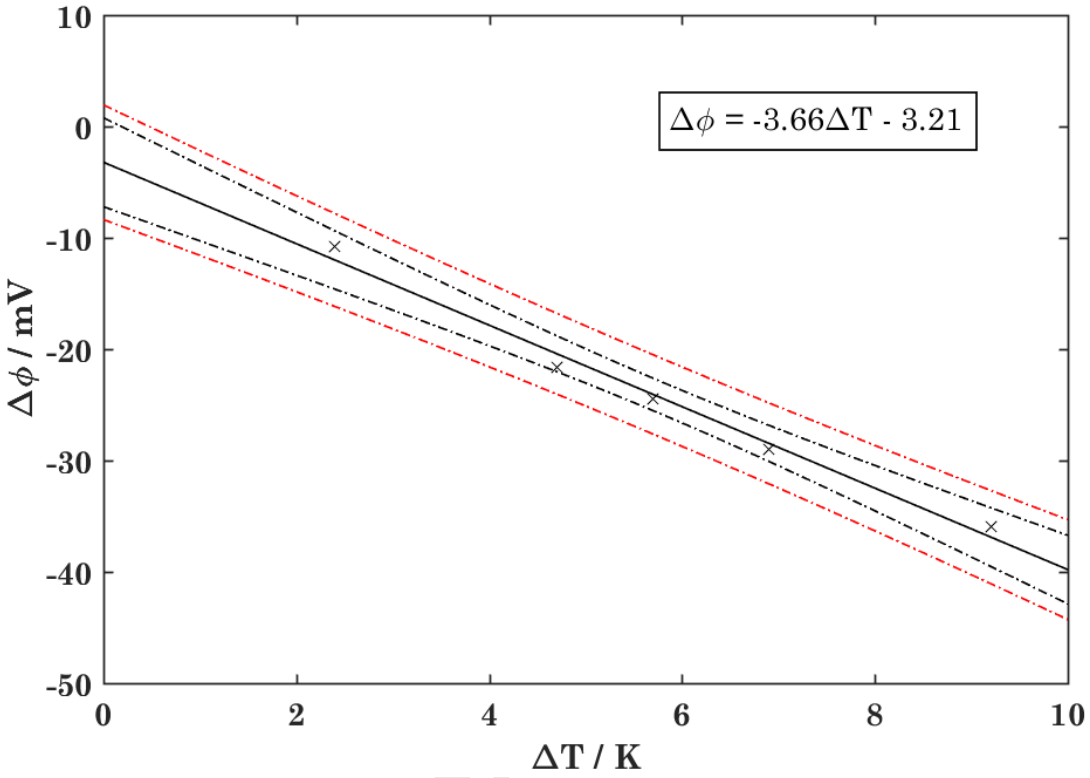

Figure 9: The emf of a cell with $LiFePO_4$ electrodes vs the temperature difference applied to the cell. The fit to a straight line is shown with 95% confidence. Prediction intervals (red line) are also shown.

5.3. Understanding the Seebeck coefficients, in the absence and presence of Soret equilibrium

The properties that can be derived from the experimental results will allow us to model thermal phenomena in a Li-battery with greater precision, on shorter and longer time-scales. We discuss now the time-dependent phenomena (electrolyte diffusion), before we discuss the contributions to the Seebeck coefficients. The effective diffusion coefficients of the Li-salt and DEC are shown in Table 1. Self diffusion coefficients in the order 10^{-10} m^2s^{-1} have been measured for both the carbonates and the salt in bulk solutions [30]. This indicates that one component is affected by the separator porosity. We have here stipulated that it is the carbonates that are affected by this, due to the fact that both carbonate molecules are bulky. Further work must be done to determine this however.

The relaxation times according to de Groot [22], θ_1 and θ_2, defined by equation 56, are 10 and 910 minutes, respectively. The diffusion coefficients differ also by about two orders of magnitude. Clearly, it is a good approximation to consider the development of the Soret equilibrium of the Li-salt, independent of that of the DEC. The characteristic times are relevant for the charging or discharging processes of a battery with such electrolytes. The first Soret equilibrium can well be reached within a reasonable charging time (within an hour), but not the second one. That is so slow, that it is likely not reachable in practice. It does however pinpoint the fact that concentration gradients in the electrolyte can have an impact on the local heat production, as will be further discussed below.

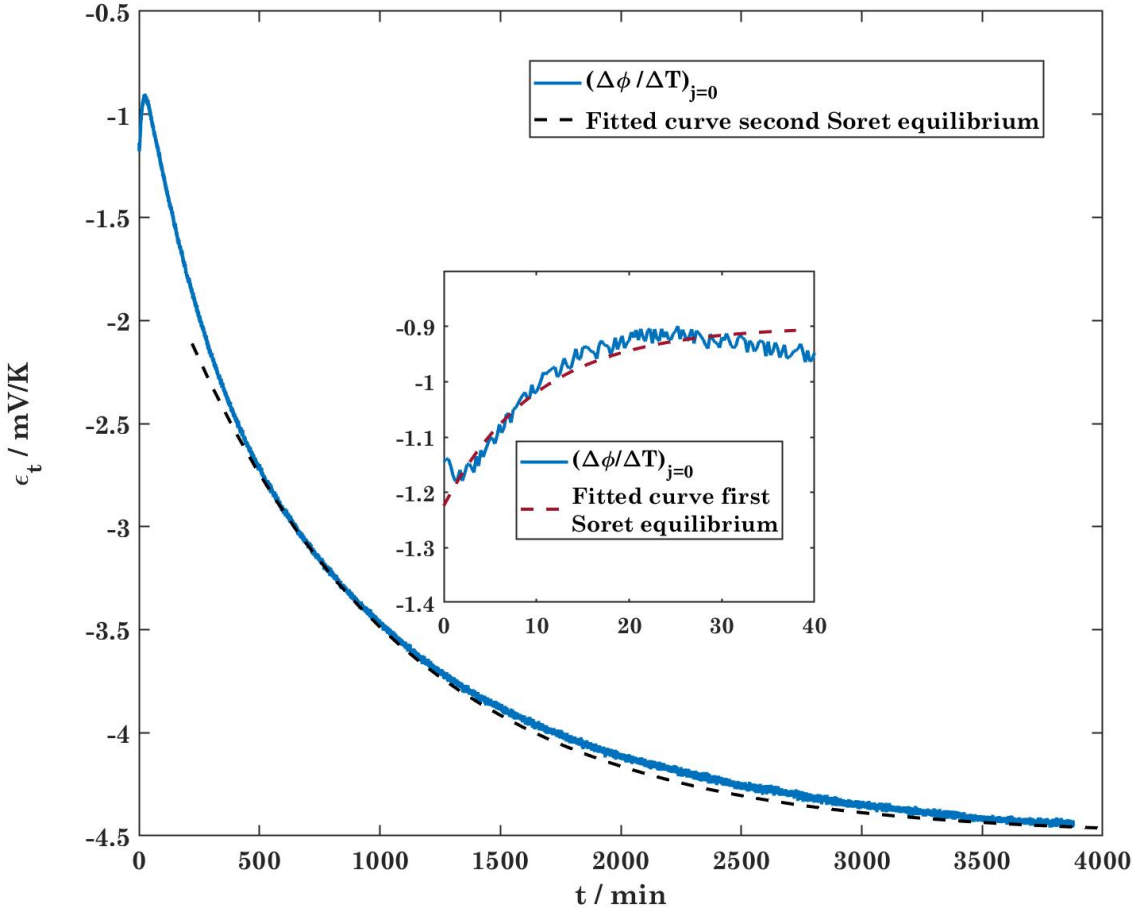

Figure 10: The thermoelectric potential as a function of time, and its fit to Eqs. 57 and 58 containing the development to the Soret state for two independent diffusional processes. The temperature difference between the electrodes were ΔT = 2.4 K.

Table 1: Characteristic times and diffusion coefficients obtained from emf- measurement in cells with $LiFePO_4$ electrodes. Errors from the fit to the theoretical curve (Eq. 57-58) are given with two standard deviations.

θ_1 / min	θ_2 / min	D_1^{eff} /m^2 s^{-1}	D_2^{eff} / m^2 s^{-1}
10	910	$(4 \pm 3) \cdot 10^{-10}$	$(5.9 \pm 0.6) \cdot 10^{-12}$

Table 2: The stationary state thermoelectric potential at uniform electrolyte ($\epsilon_{t=0}$), and at partial ($\epsilon_{t=\text{int}}$) and full Soret equilibrium ($\epsilon_{t=\infty}$). The determination from experiments is explained in the text. Errors are given as two standard deviations in the curve fits.

ΔT /K	$\epsilon_{t=0}$ /mV K^{-1}	$\epsilon_{t=\text{int}}$ /mV K^{-1}	$\epsilon_{t=\infty}$ /mV K^{-1}
2.4	-1.1 ± 0.2	-1.0 ± 0.2	-4.5 ± 0.2
4.7	-1.1 ± 0.4	-0.8 ± 0.4	-4.6 ± 0.4
5.7	-1.3 ± 0.4	-1.0 ± 0.4	-4.3 ± 0.4
6.9	-1.4 ± 0.2	-0.9 ± 0.2	-4.2 ± 0.2
9.2	-1.6 ± 0.4	-1.0 ± 0.4	-3.9 ± 0.4
Average	-1.3 ± 0.4	-0.9 ± 0.2	-4.3 ± 0.6

All Seebeck coefficients of Table 2 are negative. This means that heat is transported from the low to the high temperature end of the cell when charge is transported from left to right in the outer circuit of the cell. It also means that the process lowers the battery voltage, when in operation. Power is used to move heat "uphill" and separate components. A negative Seebeck coefficient gives a positive Peltier heat. This means that $LiFePO_4$ when it functions as an anode will be a heat sink, while it is a heat source during discharging (when it functions as a cathode).

The origin of the sign can be explained by Eq. 61 for the final Soret equilibrium state. The value of the transported entropy of electrons $S^*_{e^-}$ is in general small, while the entropy of lithium metal is 29 J/K mol [29]. The entropy of intercalated Li could be higher than of the pure lithium metal. The only thing we know of the transported entropy of Li^+, $S^*_{Li^+}$ is its sign, which is positive. The reason why the Seebeck coefficient has a negative sign, must therefore be that $S^*_{Li^+} > S_{Li}$. By the same argument the values reported by Huang *et al.*, Kuzminskii *et al.* and Black *et al.* must have a negative sign for $S^*_{Li^+}$ to be positive [12, 15, 16]. The fact that the absolute value of $\epsilon_{t=0}$ is smaller than the absolute value of $\epsilon_{t=\infty}$, is due to the contributions from the heats of transfer. This is a large contribution. Structural changes may change the value for the transported entropy and molar entropy of Li as well, and contribute to errors in the observation.

Due to the time needed to reach a defined temperature profile, the initial values have a larger uncertainty than the values at Soret equilibrium. Diffusion may likely start before the response of the system to the temperature difference. The initial Seebeck coefficient will then be underestimated. A way to confirm this would be to accurately measure the heats of transfer, q^* and calculate the initial effect.

5.4. Half cell Peltier heats

The Seebeck coefficient gives direct access to the half cell Peltier heat, as described in the theoretical section. The Peltier heats of the $LiFePO_4$-electrode compartments were computed form Eq.3. They are given in Table 3.

Knowing the value of one half cell, we can compute any other half cell-value, if we also know the cell's total entropy change. The Peltier heat of the graphite electrode, denoted C_6 was calculated is this manner, using the entropy change of the Li_xC_6 || Li_xFePO_4 cell during charging. As average value for the entropy change, we used $\Delta S = -60\pm 15$ J/mol K (for $x = 1$ in Li_xFePO_4, and $x = 0$ in Li_xC_6), see Viswanathan *et al.* [8]. The results of these computations are also given in Table 3.

Table 3: Peltier heats for the lithium iron phosphate electrode and graphite electrode in a battery with electrolyte of 1 M lithium hexafluorophosphate in EC:DEC = 50:50 w% (see text).[a]

	Peltier heat /kJ mol^{-1}		
	Homogeneous solution	Partial Soret equilibrium	Soret equilibrium
Electrode	$t = 0$	$t = \text{int}$	$t = \infty$
$LiFePO_4$	37 ± 9	26 ± 6	122 ± 12
C_6	19 ± 13	8 ± 10	104 ± 16

[a] In a prelimenary report we used a different sign convention [18]. The values reported here are in agreement with the convention in Eq. 1 and in Førland *et al.* [9].

The values in Table 3 are all substantial when compared for instance with the enthalpy of evaporation of water (44 kJ/mol [29]). Again, the positive values for the $LiFePO_4$-electrode mean that heat is absorbed in the electrode region, when it functions as an anode (during discharging). Equivalently for the graphite electrode, the positive value means that the electrode region is a heat sink during charging when it functions as a cathode, and a heat source during discharging when it functions as an anode. In [18] we used the average entropy change to calculate the Peltier heat of graphite. If, however, we use the entropy at 0% state of charge we get, for a measured initial Peltier heat of $LiCoO_2$ of 84±9 kJ/mol, 53±9 kJ/mol for graphite (using $T\Delta S$ =32 kJ/mol, [8], and the sign convention used in this paper).

Visvanathan *et al.* reported the value of $T\Delta S$ for a battery cell, equal to 18 kJ/mol at 298 K during charging. This represents only half the heat absorbed at the cathode during charging. The heat released at the anode is of the same magnitude. Usually in thermal modeling it is assumed that $T\Delta S$ is absorbed uniformly across the cell. It is clear from these numbers that this assumption is wrong. There is a large asymmetry of where the reversible heat is absorbed and released in the cell. It will be interesting to include the new local values in a future thermal modeling of the cell.

The ϵ-value of Huang *et al.* corresponds to a Peltier heat of 34 kJ/mol (were we have changed their sign convention so that $S^*_{Li^+}$ is positive). Such a value is significant, compared to the overall reversible heat effect, computed from the entropy change. An ϵ-value has also been computed when different electrodes are used [8]. These measurements cannot be used to find single electrode heats. Huang *et al* calculated the Peltier heat of the Li_xCoO_2 (36 kJ/mol) and of the graphite electrode (27 kmol/mol) at 100% state of charge in this manner. The results mean that $LiCoO_2$ acts as a heat source during discharging and a heat sink during charging. The reverse is true for the graphite electrode. The authors concluded, in agreement with the results presented here, that local reversible heat effects were not negligible [12].

The contribution from the electrolyte to the Seebeck coefficient changes when concentration gradients are present in the cell. Which Peltier heat to use in thermal modeling will then depend on whether any concentration gradients are present in the battery. An accurate thermal model should therefore also account for the concentration profiles in the cell. Independent determinations of $t_1q_1^*$ and $t_2q_2^*$ in Equation 59 are needed to find the Peltier heat at a given concentration gradient. Additional knowledge, i.e. of the heats of transfer, provides a time-dependent expression for the thermal signature of an electrode. As can be seen from Equations 59-61, we may estimate these terms from the values of the thermoelectric potential at initial times, first Soret equilibrium. We choose not to do so, because of the high uncertainty involved, leaving it to future work.

6. Conclusion

We have documented by theory and experiments that there are large local reversible heat effects in the electrode compartments of batteries with electrodes of $LiFePO_4$ and graphite. The Peltier heats vary from 37 to 122 or 19 to 104 kJ/mol, respectively. Under reversible discharge at 0% state of charge the cathode is exothermic and the anode endothermic and vice versa while charging. The theoretical derivations are lengthy, but few principles are involved. Once the entropy production is formulated, the equations of transport are defined in a systematic manner. They can all be related to measurements, and are in fact needed to describe all coupled transport phenomena.

A selection of coefficients are reported here; prominently the main diffusion coefficients and the Peltier heats. The Peltier heats reported in this work are of the same order of magnitude as those reported by Huang *et al.* for $LiCoO_2$ electrodes. The Peltier heat calculated for graphite was in good agreement with the value reported for the graphite anode by these authors. We have, however, added more details to their picture of the battery, through the theoretical analysis of the time-dependence of the Seebeck coefficient, and through the accompanying experiments.

We have only investigated one system at one state of charge. The effect of the various states of charge should be investigated. These data might help us to improve on thermal models of the battery.

Acknowledgment

The authors A.F.G, S.K and D.B are grateful to the Center of Excellence Funding Scheme from the Norwegian Research Council, PoreLab project no. 262644. All authors are grateful to ENERSENSE. The group of authors acknowledge the Research Council of Norway (RCN) (project no. 228739), for funding through the project "Life and Safety for Li-ion batteries in Maritime conditions (SafeLiLife)".

References

[1] D. H. Doughty, E. P. Roth, A General Discussion of Li-Ion Battery Safety, The Electrochemical Society Interface 21 (2) (2012) 37–44. arXiv:http://interface.ecsdl.org/content/21/2/37.full.pdf+html, doi:10.1149/2.F03122if.

[2] J. Fan, S. Tan, Studies on Charging Lithium-Ion Cells at Low Temperatures, Journal of The Electrochemical Society 153 (6) (2006) A1081–A1092. doi:10.1149/1.2190029.

[3] T. Waldmann, M. Wilka, M. Kasper, M. Fleischhammer, M. Wohlfahrt-Mehrens, Temperature dependent ageing mechanisms in Lithium-ion batteries – A Post-Mortem study, Journal of Power Sources 262 (2014) 129 – 135. doi:https://doi.org/10.1016/j.jpowsour.2014.03.112.

[4] E. Thomas, H. Case, D. Doughty, R. Jungst, G. Nagasubramanian, E. Roth, Accelerated power degradation of Li-ion cells, Journal of Power Sources 124 (1) (2003) 254 – 260.

[5] H. Liu, Z. Wei, W. He, J. Zhao, Thermal Issues About Li-ion Batteries and Recent Progress in Battery Thermal Management Systems: A Review, Energy Conversion and Management 150 (Supplement C) (2017) 304 – 330. doi:https://doi.org/10.1016/j.enconman.2017.08.016.

[6] T. M. Bandhauer, S. Garimella, T. F. Fuller, A Critical Review of Thermal Issues in Lithium-Ion Batteries, Journal of The Electrochemical Society 158 (3) (2011) R1–R25. doi:10.1149/1.3515880.

[7] G. Xia, L. Cao, G. Bi, A review on battery thermal management in electric vehicle application, Journal of Power Sources 367 (2017) 90–105.

[8] V. V. Viswanathan, D. Choi, D. Wang, W. Xu, S. Towne, R. E. Williford, J.-G. Zhang, J. Liu, Z. Yang, Effect of Entropy Change of Lithium Intercalation in Cathodes and Anodes on Li-ion Battery Thermal Management, Journal of Power Sources 195 (11) (2010) 3720 – 3729. doi:http://dx.doi.org/10.1016/j.jpowsour.2009.11.103.

[9] K. S. Førland, T. Førland, S. K. Ratkje, Irreversible thermodynamics : theory and applications, John Wiley & Sons Inc, 1988.

[10] S. K. Ratkje, Local heat changes during aluminium electrolysis, Electrochimica Acta 36 (3) (1991) 661 – 665. doi:https://doi.org/10.1016/0013-4686(91)85155-Z.

[11] L. Rao, J. Newman, Heat-Generation Rate and General Energy Balance for Insertion Battery Systems, Journal of The Electrochemical Society 144 (8) (1997) 2697–2704. doi:10.1149/1.1837884.

[12] Q. Huang, M. Yan, Z. Jiang, Thermal study on single electrodes in lithium-ion battery, Journal of Power Sources 156 (2) (2006) 541 – 546.

[13] S. de Groot, P. Mazur, Non-equilibrium Thermodynamics, Dover Books on Physics, Dover Publications, 1984.

[14] S. Kjelstrup, D. Bedeaux, Non-Equilibrium Thermodynamics of Heterogeneous Systems, World Scientific Publishing Co. Pte. Ltd., 2008.

[15] Y. Kuzminskii, V. Zasukha, G. Kuzminskaya, Thermoelectric Effects in Electrochemical Systems. Nonconventional Thermogalvanic Cells, Journal of Power Sources 52 (2) (1994) 231 – 242. doi:https://doi.org/10.1016/0378-7753(94)02015-9.

[16] J. J. Black, J. B. Harper, L. Aldous, Temperature effect upon the thermoelectrochemical potential generated between lithium metal and lithium ion intercalation electrodes in symmetric and asymmetric battery arrangements, Electrochemistry Communications 86 (2018) 153 – 156. doi:https://doi.org/10.1016/j.elecom.2017.12.005.

[17] J. N. Agar, In: P. Delahay, (Ed.), Advances in Electrochemistry and Electrochemical engineering, Vol. 3, Thermogalvanic Cells, Interscience, New York, 1963.

[18] F. Richter, A. Gunnarshaug, O. S. Burheim, P. J. S. Vie, S. Kjelstrup, Single Electrode Entropy Change for $LiCoO_2$ Electrodes, ECS Transactions 80 (10) (2017) 219–238.

[19] T. Zhang, D. Li, Z. Tao, J. Chen, Understanding Electrode Materials of Rechargeable Lithium Batteries via DFT Calculations, Chinese Materials Research Society 23 (2013) 256–272.

[20] W. Gu, C. Wang, Thermal-electrochemical modeling of battery systems, Journal of The Electrochemical Society.

[21] J. N. Agar, W. G. Breck, Thermal Diffusion in Non-Isothermal Cells: Part 1.-Theoretical Relations and Experiments on Solutions of Thallous Salts, Transactions of the Faraday Society 53 (1957) p. 67.

[22] S. de Groot, Théorie Phénoménologique De L'effet Soret, Physica 9 (7) (1942) 699 – 708. doi:https://doi.org/10.1016/S0031-8914(42)80036-1.

[23] M. T. Børset, X. Kang, O. S. Burheim, G. M. Haarberg, Q. Xu, S. Kjelstrup, Seebeck Coefficients of Cells with Lithium Carbonate and Gas Electrodes, Electrochimica Acta 182 (Supplement C) (2015) 699 – 706. doi:https://doi.org/10.1016/j.electacta.2015.09.091.

[24] I. Prigogine, Etude thermodynamique des phénomènes irréversibles (1947).

[25] J. A. Bierlein, A Phenomenological Theory of the Soret Diffusion, The Journal of Chemical Physics 23 (1) (1955) 10–14. doi:10.1063/1.1740504.

[26] W. J. Ullman, R. C. Aller, Diffusion coefficients in nearshore marine sediments1, Limnology and Oceanography 27 (3) (1982) 552–556. doi:10.4319/lo.1982.27.3.0552.

[27] H. J. V. Tyrrell, Diffusion and Heat Flow in Liquids, Butterworths, London, 1961.

[28] F. Richter, S. Kjelstrup, P. J. Vie, O. S. Burheim, Thermal Conductivity and Internal Temperature Profiles of Li-ion Secondary Batteries, Journal of Power Sources 359 (2017) 592 – 600. doi:https://doi.org/10.1016/j.jpowsour.2017.05.045.

[29] G. Aylward, T. Findlay, SI Chemical Data, 6th Edition, Wiley.

[30] K. Hayamizu, Temperature dependence of self-diffusion coefficients of ions and solvents in ethylene carbonate, propylene carbonate, and diethyl carbonate single solutions and ethylene carbonate+ diethyl carbonate binary solutions of LiPF6 studied by NMR, Journal of Chemical & Engineering Data 57 (7) (2012) 2012–2017.

Appendix A.

By using Gibbs-Duhem (see Eq. 35), we can eliminate $\partial c_3/\partial x$ in Eq. 44. The chemical potentials of component 1 and 2 are therefore expressed as linear combinations of $\partial c_1/\partial x$ and $\partial c_2/\partial x$ in Eq. 46. The coefficients a_{ij} are given by:

$$\begin{aligned}
\frac{\partial \mu_{1,T}}{\partial x} =& \left(\Gamma_{11} - \Gamma_{13}\frac{\left(\Gamma_{31} + \frac{c_1}{c_3}\Gamma_{11} + \frac{c_2}{c_3}\Gamma_{21}\right)}{\left(\Gamma_{33} + \frac{c_1}{c_3}\Gamma_{13} + \frac{c_2}{c_3}\Gamma_{23}\right)}\right)\frac{RT}{c_1}\frac{\partial c_1}{\partial x} \\
&+ \left(\Gamma_{12} - \Gamma_{13}\frac{\left(\Gamma_{32} + \frac{c_1}{c_3}\Gamma_{12} + \frac{c_2}{c_3}\Gamma_{22}\right)}{\left(\Gamma_{33} + \frac{c_1}{c_3}\Gamma_{13} + \frac{c_2}{c_3}\Gamma_{23}\right)}\right)\frac{RT}{c_2}\frac{\partial c_2}{\partial x} \\
=& a_{11}\frac{\partial c_1}{\partial x} + a_{12}\frac{\partial c_2}{\partial x} \\
\frac{\partial \mu_{2,T}}{\partial x} =& \left(\Gamma_{21} - \Gamma_{23}\frac{\left(\Gamma_{31} + \frac{c_1}{c_3}\Gamma_{11} + \frac{c_2}{c_3}\Gamma_{21}\right)}{\left(\Gamma_{33} + \frac{c_1}{c_3}\Gamma_{13} + \frac{c_2}{c_3}\Gamma_{23}\right)}\right)\frac{RT}{c_1}\frac{\partial c_1}{\partial x} \\
&+ \left(\Gamma_{22} - \Gamma_{23}\frac{\left(\Gamma_{32} + \frac{c_1}{c_3}\Gamma_{12} + \frac{c_2}{c_3}\Gamma_{22}\right)}{\left(\Gamma_{33} + \frac{c_1}{c_3}\Gamma_{13} + \frac{c_2}{c_3}\Gamma_{23}\right)}\right)\frac{RT}{c_2}\frac{\partial c_2}{\partial x} \\
=& a_{21}\frac{\partial c_1}{\partial x} + a_{22}\frac{\partial c_2}{\partial x}
\end{aligned} \tag{A.1}$$

Author contributions

Original manuscript: A.F.G. performed the experiments. F. R. made the cells. A. F. G., S. K. and D. B. derived the theory. A. F. G. and S. K. wrote the manuscript. O. B. helped design the experiments, provided feedback on the experiments and reviewed the manuscript. All authors contributed to the discussions. All authors approved the final formulations.

Revised manuscript: A. F. G., S. K., D. B. and O. B. discussed the revisions, A. F. G, D.B and S. K. reviewed and edited the manuscript.

Declaration of interests

☒ The authors declare that they have no known competing financial interests or personal relationships that could have appeared to influence the work reported in this paper.

☐The authors declare the following financial interests/personal relationships which may be considered as potential competing interests: